Author/s:
Shepherd, TJ;Walsh, KJ

Title:
Sensitivity of hurricane track to cumulus parameterization schemes in the WRF model for three intense tropical cyclones: impact of convective asymmetry

Date:
2017-08-01

Citation:
Shepherd, T. J. & Walsh, K. J. (2017). Sensitivity of hurricane track to cumulus parameterization schemes in the WRF model for three intense tropical cyclones: impact of convective asymmetry. Meteorology and Atmospheric Physics, 129 (4), pp.345-374. https://doi.org/10.1007/s00703-016-0472-y.

Persistent Link:
https://hdl.handle.net/11343/282723

Sensitivity of hurricane track to cumulus parameterization schemes in the WRF model for three intense tropical cyclones: Impact of convective asymmetry.

TRISTAN J. SHEPHERD

SCHOOL OF EARTH SCIENCES, UNIVERSITY OF MELBOURNE, MELBOURNE, VICTORIA, AUSTRALIA

KEVIN J. WALSH*

SCHOOL OF EARTH SCIENCES, UNIVERSITY OF MELBOURNE, MELBOURNE, VICTORIA, AUSTRALIA

SUBMITTED TO METEOROLOGY AND ATMOSPHERIC PHYSICS

[MARCH 2016]

**Corresponding author address*: Kevin J. Walsh, School of Earth Sciences, University of Melbourne, Victoria 3010, Australia

E-mail: kevin.walsh@.unimelb.edu.au, Phone: +61-3-8344-6523, Fax: +61-3-8344-7761.

ABSTRACT

This study investigates the effect of the choice of convective parameterisation (CP) scheme on the simulated tracks of three intense tropical cyclones (TCs), using the Weather Research and Forecasting (WRF) model. We focus on diagnosing the competing influences of large-scale steering flow, beta drift and convectively-induced changes in track, as represented by four different CP schemes (Kain-Fritsch (KF), Betts-Miller-Janjic (BMJ), Grell-3D (G-3), and the Tiedtke (TD) scheme). The sensitivity of the results to initial conditions, model domain size and shallow convection is also tested.

We employ a diagnostic technique from Chan et al. (2002) that separates the influence of the large-scale steering flow, beta drift and the modifications of the steering flow by the storm-scale convection. The combined effect of the steering flow and the beta drift causes TCs typically to move in the direction of the wavenumber-1 (WN-1) cyclonic potential vorticity tendency (PVT). In instances of asymmetrical TCs, the simulated TC motion does not necessarily match the motion expected from the WN-1 PVT due to changes in the convective pattern. In the present study, we test this concept in the WRF simulations and investigate whether if the diagnosed motion form the WN-1 PVT and the TC motion do not match, this can be related to the emerging evolution of changes in convective structure.

Several systematic results are found across the three cyclone cases. The sensitivity of TC track to initial conditions (the initialisation time and model domain size) is less than the sensitivity of TC track to changing the CP scheme. The simulated track is not overly sensitive to shallow convection in the KF, BMJ, and TD schemes, compared to the track difference between CP schemes. The G3 scheme, however, is highly sensitive to shallow convection being used. Furthermore, while agreement between the simulated TC track direction and the WN-1 diagnostic is usually good, there are important periods of differences that are often associated with model-generated convective asymmetries.

1. Introduction

Moist convection varies widely in scale but is important for driving global scale atmospheric processes. Deep convective clouds have the ability to influence atmospheric processes and tropical cyclones (TCs) are extreme examples of deep moist convection. Moist convection must be represented accurately in atmospheric models for successful representation of dynamical/physical processes. Since this convection comprises very small-scale mixtures of updrafts and downdrafts, it is computationally expensive to represent these processes directly. Thus these processes must be parameterized in order to achieve accurate representation of moist convection. Stensrud (2007) argues that the grid spacing needed to resolve individual convective elements is likely to be between 25 and 1000 m and thus the realistic computational requirements needed to run routinely true convective resolving simulations lie in the future. Currently, most research and operational TC models are able to successfully employ resolutions of about 1 km (at convection-permitting resolutions), which is still too coarse for accurate treatment of subgrid scale processes (e.g. updrafts and downdrafts in convection-resolving simulations).

Convection is often parameterized in models through a cumulus parameterization (CP) scheme. A CP scheme must account for the rate of subgrid precipitation, latent heat release and redistribution of the thermodynamic and dynamic variables (such as heat and moisture) in the vertical as a result of convection (e.g Kain and Fritsch 1990). There are indications that it is possible to switch off CP at grid resolutions less than 4 km and allow an explicit microphysics scheme to resolve cloud and precipitation processes (Weisman et al. 1997). Horizontal resolutions around 4 km are often termed the “grey area” because at this scale a parameterisation of deep convection may be problematic, as convection is partly resolved and partly subgrid. On scales of 10 – 50 km, however, the model still requires a CP scheme to accurately represent the subgrid scale processes. Thus for multiply-nested mesoscale models it has become a recent practice to use CP on the coarse outer domain (e.g. 12 km resolution) and use explicit microphysics for high resolution inner nests (e.g. 4km resolution and finer), as used in Davis and Bosart (2002). Many CP schemes have been developed or modified over the past three decades (e.g. Ooyama 1971; Kuo 1974; Arakawa and Schubert 1974; Fritsch and Chappell 1980; Bougeault 1985; Betts 1986; Betts and Miller 1986; Frank and Cohen 1987; Tiedtke 1989; Gregory and Rowntree 1990; Emanuel 1991; Kain and Fritsch 1990; 1993; Kain 2004; Grell 1993; Grell and Devenyi 2002; Grell et al. 2013). The problem of CP was previously reviewed by Frank (1983) and Molinari and Dudek (1992). Arakawa (2004) and Stensrud (2007) have presented the most recent review of the CP problem, while others (e.g. Nasrollahi et al. 2012) have provided updates on specific topics.

A number of studies have examined the effect of the representation of convection on TC track. Dengler and Reeder (1997) found that relatively minor changes to the CP can have a large effect on the motion of a vortex, by changing the structure of the upper-level vortex and thereby altering the steering currents across the storm vortex. Prater and Evans (2002) note that the depth of the vortex can be altered by the choice of the convection scheme, with a scheme that produces a more elevated heating profile thereby responding to a deeper layer of mean steering currents, thus altering the storm direction. Srinivas et al. (2007) and Li and Pu (2009) demonstrated the sensitivity of storm track to the choice of convection scheme and also to the specification of the boundary layer physics within the model. Nasrollahi et al. (2012) examined the sensitivity of track to various combinations of CP schemes and cloud microphysics parameterizations, finding in their case that the Betts-Miller-Janjic parameterization gave the most accurate track. Sun et al. (2014) also showed the relationship between upper-level heating caused by differences in CP and the resulting changes in the steering flow of the storm through heating-induced changes in the geopotential height.

The role of shallow convection in hurricane track and intensity prediction has also been explored. Shallow convection influences the boundary layer depth, temperature, moisture, cloud cover and winds (Bretherton et al. 2004; Kain 2004; Wang et al. 2004a,b; de Szoeke et al. 2006) and provides a pre-condition for deep convection to occur. The shallow component of a CP scheme will moisten the region above the boundary layer (up to about 600 hPa) and will modify the flow coming into the TC environment (Jimy Dudhia Pers. Comm., 2014.). Therefore, we should expect TC track sensitivity between simulations that use or do not use shallow convection, and between the use of different schemes, as each CP scheme represents shallow convection differently (see Table 1). In the present study, we aim to test this by showing track comparisons between simulations using no shallow convection and full convective cases.

In previous studies, Emanuel (1989) used an axisymmetric model to show that shallow convective clouds help to prevent overheating in the outer regions of a TC. In addition, low θ_e air is imported into the subcloud layer, which helps to cool the vortex, and leads to subsequent decay. In a 3D TC model developed by Zhu et al. (2001), Zhu and Smith (2002) explore the impact of shallow convection on the dynamics of TC intensification. They showed how shallow convection was able to stabilise the vortex core region, reducing the deep convective mass flux and buoyancy due to decreased rates of heating and drying in the troposphere. The diminished buoyancy in the vortex core decreased the vortex intensification rate. Using the Florida State University Global Spectral Model (Krishnamurti et al. 1998), O'Shay and Krishnamurti (2004) showed incremental improvement in TC track forecasts when shallow convection was included in the simulations. In a revision of convection and vertical diffusion schemes in the NCEP GFS model (Environmental Modeling Center, 2003), Han and Pan (2011) showed that using a new shallow convection scheme with a mass flux parameterisation, a decrease in TC track forecast errors resulted. This was attributed to an improvement in wind profiles, driven by heating throughout the convection layers, rather than cooling above and heating below, which the old turbulent-diffusion based shallow scheme produced. Torn and Davis (2012) showed an improvement in TC track forecasts when using the Tiedtke CP scheme compared to the Kain-Fritsch scheme. They stated the Tiedtke scheme allows for more appropriate treatment of oceanic shallow convection due to a more active shallow convection scheme than that in Kain-Fritsch. There was a 1 K temperature bias at 700 hPa in the Kain-Fritsch simulations not present in the Tiedtke simulations, attributed to a lack of shallow convection in Kain-Fritsch. This generated horizontal temperature gradients associated with the wind biases affecting the TC tracks simulated with the Kain-Fritsch scheme.

While it is clear that differences in the simulation of convection can cause differences in track, here we present a detailed analysis of the effect of the choice of CP scheme on the simulated tracks of three intense tropical cyclones. Our focus will be on diagnosing the competing influences of large-scale steering flow, beta drift and convectively-induced changes in track, as represented by four different CP schemes. The sensitivity of the results to initial conditions, model domain size and shallow convection is also tested. The Weather Research and Forecasting (WRF) model (Skamarock et al. 2008) is used in this study. The WRF model is suitable for simulating hurricanes because of its full physics and 3D grid structure. While WRF has been widely employed for hurricane research (e.g. Davis et al. 2008; Hill and Lackmann 2009; Fovell et al. 2009; Cao et al. 2011; Kumar et al. 2011; Kieu et al. 2012; Cha and Wang 2013), sensitivity studies using it to examine the impact of CP differences on hurricane track and intensity are few. We present a range of WRF simulations from one North American case, one North West Pacific case and one Australian case. We find that sensitivity of TC track to initial conditions (initialisation time and model domain size) is considerably less than the sensitivity of TC track to the changing of CP scheme; the

TC track is not particularly sensitive to shallow convection in the Kain-Fritsch, Betts-Miller-Janjic and Tiedtke schemes (see section 2 for descriptions of these parameterizations), but TC track is highly sensitive in the G3 scheme; and the G3 simulation with shallow convection consistently performed poorly across all three cyclone cases. Section 2 outlines the methods used. The cases are outlined in section 3. The results are presented in section 4 and discuss track and intensity sensitivity to changes in CP scheme, and the physical mechanisms for this sensitivity. We then summarise this work by placing it in context of other studies on TC motion and CP sensitivity.

2. Methodology

2.1. Model and domain specification

The version of WRF used here is v3.3.1 (Skamarock et al. 2008). An experimental design is used to eliminate other factors which may cause model simulation sensitivity to something other than CP specification (e.g. initial condition error). Two criteria were selected to test the initial condition sensitivity: initialization time and model domain size. To test the sensitivity of the track simulation to initial conditions, we conduct the same simulations but initialised 6 hours later. To estimate the sensitivity due to lateral boundary conditions, we conduct the same simulations maintaining the inner-nest dimensions, but use a smaller outer coarse domain (see Fig. 1). For these tests, all physics parameterisations and other model settings remain identical and only the CP is changed.

In order to make some general conclusions about the CP schemes, a selection of three, well-simulated category 4 or 5 hurricanes from different basins are chosen as case studies. These storms were Rita (2005), Megi (2010) and Yasi (2011) (see section 3). There are a total of 16 simulations for each cyclone case. Four CPs are tested (and summarised in Table 1): Kain-Fritsch (KF) (Kain and Fritsch 1990; 1993; Kain 2004), Betts-Miller-Janjic (BMJ)

(Betts 1986; Betts and Miller 1986; Janjic 1994), Grell-3D (G3) (Grell and Devenyi 2002), and Tiedtke (TD) (Tiedtke 1989; Zhang et al. 2011). Simulations which are denoted '+6' and 'dom2' explore the initial condition uncertainty: the '+6' simulations are initialised 6 hours later and the 'dom2' simulations use a different domain size. A separate set of experiments denoted 'NO_SHALLOW' (hereafter NS) explore the sensitivity of track and intensity when the shallow convection component of each CP scheme is turned off. The purpose of these tests is to ascertain the role of shallow convection and whether the shallow convection processes modify the environment, or whether it is the deep convection controlling the large scale. Note that in the case of the G3 scheme, shallow convection is not included by default; the user must activate a switch to run shallow convection with this scheme. Thus, simulations denoted G3_NS are the default configuration of the scheme, whereas those denoted G3 will have shallow convection included.

The physics options used in all the experiments were the MYJ PBL scheme (Mellor and Yamada 1982; Janjic 1990; Janjic 2001), the Eta microphysics scheme (Rogers et al. 2001), the rapid radiative transfer model (RRTM) for longwave radiation (Mlawer et al. 1997), the Dudhia scheme for shortwave radiation (Dudhia 1989), and the Monin-Obukhov (Janjic Eta) surface layer scheme (Janjic 1996; 2001). The domain configuration for the standard simulations (dom1) is shown in Fig. 1. The parent (i.e. outer) domain has a resolution of 12 km and 423 x 324 grid points and the inner movable nests are 4 km and 1.33 km with 201 x 201 and 240 x 240 grid points respectively. Note that the 'dom2' experiments have the same nest dimensions, but an outer domain of 380 x 280 grid points. The model has 33 vertical levels with a top of 50 hPa. Initial and boundary conditions for the large-scale atmospheric fields were derived from 1° x 1° NCEP Global Final Analysis (FNL) data (National Centers for Environmental Prediction/National Weather Service/NOAA/U.S. Department of Commerce, 2000). The model was updated with FNL data every 6 hours. Nest positions were updated every 15 minutes using an automatic vortex-following algorithm which tracked the centre of the vortex at 750 hPa. One-way nesting is used, and CP is not used in the inner-nests.

2.2 Diagnostic methods

A diagnostic technique is employed that separates the influence of large-scale steering flow, beta drift and the modifications of the steering flow by storm-scale convection. For the definition of the steering flow, we use the deep-layer mean flow between 850 hPa and 200 hPa (e.g. based on Chan and Gray 1982).

The motion of a tropical cyclone deviates from the direction of the large-scale steering flow due to “beta-drift”, caused by the interaction between the vortex and the gradient of the Coriolis force (Holland 1983; Chan and Williams 1987). Wu and Wang (2000) showed that the combined effect of the steering flow and the beta drift causes tropical cyclones typically to move in the direction of the wavenumber-1 (WN-1) cyclonic potential vorticity tendency (PVT). Wu and Wang (2000) used idealised symmetric baroclinic TCs in their study. For simulations of asymmetrical TCs, however, Chan et al. (2002) showed that the diagnosed WN-1 PVT and the simulated TC motion may not match exactly, as changes in the convective pattern can lead to track oscillations and/or track changes that differ from the expected direction indicated by the PVT. In this circumstance, the motion of the TC has not yet responded to an environmental change in the PV forcing. In the present study, we test this concept in the WRF simulations and investigate whether if the diagnosed motion from the WN-1 PVT and the TC motion do not match, this can be related to the emerging evolution of changes in convective structure (see also Chan and Kepert 2010). To our knowledge, this is the first time that this diagnostic has been applied to simulations using the WRF model.

A detailed description of the diagnostic method is contained in Wu and Wang (2000) and is only briefly outlined here. In order to calculate the PVT, a 6 hour average of PV is taken around time 1 and the same is then done for time 2. The WN-1 component is then extracted for each averaged field (i.e. PV at time 1 and PV at time 2). The PVT ($\frac{\partial q_1}{\partial t}$) is then calculated. Here, the time difference between PV (time1) and PV (time2) is 6 hours (this is chosen to minimise the effect of storm movement in the domain). TC motion vectors used in the analysis are calculated over a 12 hour period. The latitude and longitude values from the model-simulated track output data are used to determine the TC motion vectors. The steering current is calculated over a 12 hour period to match the TC motion time frame. Note that there is a difference between the time intervals over which the WN-1 PVT is calculated and the steering current time frame, but tests showed little difference between 12- and 6-hour average steering currents. In instances where we have studied specific periods of interest, we calculated the TC motion over 6 hours to match the WN-1 PVT (note that the 6- and 12-hour TC motion directions also showed minimal difference). Cyclone centred composites of *u* and *v* wind fields are first derived before having the deep layer mean method applied. The vortex is removed using a standard WN-1 technique (Wu and Wang (2000); Yuqing Wang, Pers. Comm., 2013) to obtain the environment flow with the TC vortex removed. The steering vector is then determined by calculating the mean over this environment flow.

3. Cyclone Case Studies

3.1. Cyclone Yasi

Tropical cyclone Yasi (Fig. 2) occurred in the South West Pacific region from 29 January to 3 February 2011. Yasi was a category 4 cyclone on the Saffir-Simpson scale, and a category 5 in the Australian classification, and is regarded as one of the most powerful cyclones to hit the Australian coastal region of Queensland since records began. From

IBTrACS data, the maximum 10-minute sustained wind speed Yasi attained was 110 knots (estimated) and the lowest atmospheric pressure was 929 hPa. Total damage was estimated at A$800 million (Brisbane Times, 2011), with an estimate of a US$3.54 billion cost to insurers, making Yasi the costliest storm to hit the Australian coast (Reuters, 2011).

3.2. Hurricane Rita

Hurricane Rita (Fig. 2) occurred in the north Atlantic hurricane basin in September 2005. Rita was a Saffir-Simpson category 5 cyclone which followed only one month after hurricane Katrina and was responsible for 120 deaths across four US states. Rita was the fourth most intense Atlantic hurricane ever recorded and the most intense hurricane ever in the Gulf of Mexico. The maximum 10-minute sustained wind speed was 153 knots and lowest atmospheric pressure was 895 hPa. Rita was a costly hurricane: over US$12 billion in damage was reported (Knabb et al. 2006). Hurricane Rita is an important case to study due to its intensity.

3.3. Super Typhoon Megi

Super-typhoon Megi (Fig. 2) occurred in the western north Pacific hurricane basin in October 2010. Megi was a Saffir-Simpson category 5 cyclone responsible for the deaths of 69 people in Luzon, Philippines and Yilan County, Taiwan. Megi was the most intense tropical cyclone since Bess in 1982 (for wind speed) and had the lowest atmospheric pressure in the Northwest Pacific Ocean since Vanessa in 1984. The maximum 10-minute sustained wind speed Megi attained was 159 knots and the lowest atmospheric pressure was 885 hPa. Megi was one of the costliest tropical cyclones to hit the Philippines, with damage of US$107 million (National Disaster Risk Reduction and Management Council, 2010).

4. Results

This section presents simulated cyclone track results to explore whether there is sensitivity to the CP scheme. Some consideration is also given to simulated intensity sensitivity. We then explain our track sensitivity findings by showing the physical mechanisms responsible for track sensitivity.

4.1. Simulated cyclone track

4.1.1. Sensitivity to initial conditions

Two criteria were selected to test initial condition sensitivity: initialization time and model domain size. The track results of these tests can be viewed in Fig. 2. We consider each cyclone case in turn by examining the landfall distance difference in km between each simulation. We employ this metric rather than the difference between simulated and observed tracks to assess the size of these effects compared with the sensitivity to the CP scheme rather than their impact on track quality, which is discussed later.

4.1.1.1. Yasi

The landfall difference from the control simulation for each CP scheme due to the change in initialization time (designated in the tables as “vs. + 6”, column 2) varied between each scheme (Table 2). The overall average for all CP schemes was a difference of 59 km (column 2). In contrast, the average landfall difference between the CP schemes is 236 km (column 4). The tracks for storms initialised at 00Z (solid lines) and 6 hours later (06Z, dashed lines) are shown in Fig. 2a.

When the model domain size was changed (vs DOM2, column 3), the average landfall distance was 55 km, still considerably smaller than the sensitivity to the CP scheme. For the DOM2 runs, the CP sensitivity average was 172 km (column 7), 64 km less than the CP sensitivity average for the experiments run on the original domain. The tracks for storms initialised at 00Z (solid lines) and for DOM2 (dashed lines) are shown in Fig. 2b. It is clear from both the data in Table 2 and Fig. 2 that the sensitivity of track to both changes in the initial conditions and domain specification is less than the sensitivity to the specification of CP.

4.1.1.2. Rita

For Rita (Table 3), similar behaviour is seen. The average landfall distance difference for the initialisation test was 124 km (column 2). As for the Yasi case, landfall distance difference was smaller when the model domain size was changed (an average of 89 km). Unlike in Yasi, where track deviations at the start of the forecast explained the differences, in Rita the differences occur due to deviations towards the latter stages of its life cycle (see the tracks in Fig. 2d–e). Similarly to Yasi, the average landfall distance differences due to changes in the CP scheme were considerably larger, 237 km for the original domain and 258 km for the DOM2 domain.

4.1.1.3. Megi

For Megi (Table 4), unlike the Yasi and Rita cases, when the domain size was changed the average difference increased (compare columns 2 and 3). Similarly to the Yasi case, the tracks tended to deviate in the early stages of their life cycle (Fig. 2g–h). Again, though, the sensitivity to the changes in the CP scheme was considerably larger than to changes in initial conditions or domain size. Both the 00Z (338 km, column 4) and +6Z average (388 km, column 8) are greater than the initial condition average (95 km for +6Z, column 2, and 127 km for DOM2, column 3).

4.1.1.4. Summary

The simulated track is more sensitive to both changes in the initial conditions and domain specification than the sensitivity to the specification of CP. The average landfall difference increased when the CP scheme was changed compared to the difference from initialization time or model domain size change.

4.1.2. Sensitivity to shallow convection scheme

Exploring the sensitivity to the use of shallow convection determines whether it is the deep or shallow component in CPs which modifies the surrounding synoptic environment and thus influences track more. Fig. 2c, 2f, and 2i show tracks for simulations where the shallow convection component was switched off. These are compared to the tracks where both the deep and shallow operated (i.e. the normal use of CP). Each case is discussed with reference to the data in Tables 2 – 4.

4.1.2.1. Yasi

The KF, BMJ and TD schemes have virtually identical tracks to their no shallow counterparts (Fig. 2c). Indeed, the landfall distance difference between each CP case and the NS equivalent is 15, 14 and 37 km respectively (Table 2, Column 5). In contrast, the G3 simulations exhibited strong sensitivity to the use of shallow convection: the difference in landfall between G3 and G3_NS was 278 km. This meant the average across CP schemes of 86 km is inflated by this outlier. When the scheme was run normally (G3_NS), the track was more in line with that of the KF and TD schemes (compare green dash with solid yellow and red track lines in Fig. 2c). When shallow convection was used (G3), the track followed a similar path to the BMJ.

4.1.2.2 Rita

A similar result to the Yasi case is observed with the Rita simulations. Here the KF+6 v KF+6_NS, BMJ+6 v BMJ+6_NS and TD+6 v TD+6_NS simulations showed some small difference at landfall: 41, 57 and 65 km respectively (Table 3, column 5 and Fig. 2f). The same behaviour observed in the Yasi case was seen in the Rita G3 simulations, with a large difference between G3+6 and G3+6_NS of 287 km (Table 3, column 5). Once again, the G3+6_NS track is similar to the KF and TD tracks (compare green dash with red and yellow tracks in Fig. 2f), and the G3+6 is similar to the BMJ tracks at landfall. The average was 112 km, which is also inflated by the large G3 simulation difference. In this case, the average was less than that for the 00Z initial condition comparison, but more than the average for the DOM2 simulations.

4.1.2.3 Megi

As in the other two cases, the same general result is found with the Megi simulations. When shallow convection is turned on, the TD simulation once again shows a slight difference at landfall (100 km), but the KF and BMJ runs are virtually in identical landfall positions (a difference of 10 and 2 km respectively), while the G3 simulations have a much larger difference of 343 km (Table 4, column 5), and the northward drift seen in G3 is not present in G3_NS (Fig. 2i). In this instance, turning on the shallow convection scheme in G3 has caused a large change to the TC track, causing it to deviate greatly from the observed track. Another relevant track observation is that the looping of the BMJ track is removed in BMJ_NS, but there is still a notable southwest drift in both compared with the observed track (black line). The average difference is 113 km, again largely due to the large difference in the G3 simulations. This is slightly more than the difference between the 06Z initial condition simulations (95 km), but less than the difference in the DOM2 simulations (127 km).

4.1.2.4 Summary

The simulated track is not overly sensitive to shallow convection in the KF, BMJ, and TD schemes, compared to the track difference between CP schemes. This is a systematic result seen across all cyclone cases. The G3 scheme, however, is highly sensitive to the shallow convection being used. The reasons for the difference in the G3 simulations are investigated in later sections.

4.1.3. Track sensitivity to CP scheme

It is clear from the simulated track results and data in Tables 2 – 4 that there is track sensitivity to CP shown across all cyclone cases. For the purposes of comparison, treating the KF simulation as control (KF is widely used and studied in the literature, thus enabling a reference point for comparison with other studies), we are able to analyse the landfall distance difference between simulations as an example of this sensitivity. This is shown in Tables 2 – 4 (column 4, under the heading ‘*KF vs. other CPs’* [+6 in the case of Rita]). The BMJ cases and the G3 simulation tend to be the ones which differ significantly in the Yasi and Rita cases. In contrast, in these cases the KF, TD and G3_NS simulations tend to be grouped more closely (e.g. Figs. 2c and 2f). The Megi case has much more track variability (e.g. Fig. 2i): here, the G3_NS and TD were close to each other, but the KF was not grouped with them. Physical reasons for the sensitivity are discussed in section 4.3.

4.1.4. Comparison to observed best track

One means to assess the performance of the schemes is to compare landfall position between the CP scheme and the observed best track. Due to the small number of TC cases shown here, it should be noted this does not necessarily reflect the overall performance of a scheme, which would need to be assessed by a statistical analysis of dozens of TC cases. Nevertheless, a very poor simulation of track or tropical cyclone structure would be an indication of performance even in a limited set of simulations. The data comparing the difference between the simulated landfall position to the observed landfall position is given in Table 5, along with an average difference for each simulation across the three cases. This takes the landfall difference between the simulated and observed for each simulation and averages the difference across all three cyclone cases. We can then break this down for individual scheme by averaging the four runs for each scheme (i.e. average of KF, KF+6, KF_NS, KF_DOM2 across all cyclone cases) to obtain an average landfall difference across all cyclone cases according to experiment group (note that the averages for G3 are affected by the Megi simulation not making landfall). From these values we note that G3, regardless of the Megi case not making landfall, still produced the largest average difference between the simulation and observed landfall (318 km) (Table 5, row 3). In contrast, the average for G3_NS was 144 km (Table 5, row 11). The TD case had a difference of only 86 km and this is reflected throughout the other TD runs, with an overall difference average (i.e. average of TD, TD+6, TD_NS, TD_DOM2) of only 146 km, compared to KFs (245 km), BMJs (241 km) and G3s (246 km). Obviously there is substantial variability for each specific simulation/scheme between cyclone cases. Some schemes may perform better for certain cases compared to other schemes, but the averaging does tend to indicate that the TD and G3_NS simulations were particularly consistent in having low track error across all three cases. G3, however, tended to produce both variability and larger errors across all three cases. KF and BMJ tended to be somewhere in the middle.

4.2 Simulated cyclone intensity

The emphasis of this study is on the sensitivity of simulated track, but some consideration must be given to intensity also. Without reasonable intensity prediction, track comparison becomes less meaningful. Different representation of CP can also lead to dissimilar TC intensity, which can affect the TC track. Simulated intensity is compared for the initial condition and shallow CP simulations for each case.

4.2.1 Yasi

Simulated pressure differences between the 00Z and +06Z cases are shown in Fig. 3a–b. For each scheme, there is minimal separation between the 00Z and +06Z counterpart over the first 24 hours, but later into the forecast minor changes emerge. At most times after 24 hours, the difference is less than 15 hPa in all the cases, which reinforces the point regarding minimal sensitivity to initial conditions. Moreover, the variation between the schemes themselves, particularly the KF and BMJ, is more pronounced than the intensity change from changing the initial time. This confirms previous findings for the tracks, where

CP changes result in more sensitivity than changes in initial time. There is, however, little difference between the G3, TD and BMJ simulated intensity over most of the simulation period. The KF produced the deepest storm and subsequently is more separated from the other cases. Finally, in comparison to the observations, given no bogussing or other data assimilation was applied, the model does well to match intensity, especially when using the KF scheme.

The simulated wind speed is recalculated as a six hour moving average in order to observe more general trends (Fig. 3b). The wind speed rises gradually over the simulation period, consistent with a gradual spin up over the first 24 hours. The wind speed results mirror those for pressure. In comparison to observations, wind speed tends to be over-predicted in the first 24 – 36 hours, which may be a result of initialisation error.

The comparison of the shallow and NS convection cases illustrates an identical response to that seen for the tracks. The simulated pressure difference between the shallow and NS cases is minimal, except in the G3 scheme, where G3 run with shallow convection (G3) produced a much weaker storm than G3_NS (Fig. 3c). The same result is reflected in the associated wind speed (Fig. 3d).

4.2.2 Rita

Simulated pressure (Fig. 3e) shows no significant differences between the 00Z and +06Z cases, except minor separation (i.e. 5 hPa) between the G3 and G3+6 cases. Despite there being marked track sensitivity, sensitivity of simulated pressure to CP scheme is less than 20 hPa. The most significant observation here is that simulated pressure is not able to match the rapid intensification of Rita, which in the absence of bogussing, is likely a result of current model progress in parameterisation schemes, or other TC processes involved in rapid intensification, such as strong SST changes, or lack of coupling with an appropriate ocean model. Simulated wind speed, plotted as a six hour moving average (Fig. 3f) matches the findings for pressure. In contrast to Yasi, BMJ performed best here, with G3 weakest.

The use of no shallow convection has negligible effect in Rita also. Simulated pressure difference (Fig. 3g) between the two types of run is insignificant. In this cyclone case, however, despite there being substantial track difference between the G3+6 and G3+6_NS, the simulated pressure does not differ to the same degree. Only after 72 hours do the pressures begin to deviate from each other, and even then it is less than 10 hPa in difference. The six hour moving average for wind speed shows more variability between G3+6 and G3+6_NS (Fig. 3h), but this is in the latter stages of the simulation, which matches the same period for the pressure deviation. The other simulations (e.g. KF+6 vs. KF+6_NS; BMJ+6 vs. BMJ+6_NS; TD+6 vs. TD+6_NS) do not show this same separation trend as that seen between G3+6 and G3_NS+6, that is, when the +06Z is compared to the NS case, the other cases tend to show very minimal pressure and wind difference.

4.2.3 Megi

The simulated pressure for different initial conditions (Fig. 3i) shows the only case to exhibit sensitivity to initial time was G3: the G3+6 simulation is considerably weaker than the G3. There are also intensity differences between the schemes, with BMJ somewhat weaker than KF and TD. The weakening of BMJ after 48 hours is consistent with its looping track. The TD and KF cases reach an intensity of 930 hPa before stabilising. None of the cases are able to match the rapid intensification observed after 60 hours (the G3 result is not meaningful given the track was so poor). Additionally, the wind speed intensity (Fig. 3j), confirms what is seen for pressure. Simulated intensity here, however, is much greater than the observed wind speeds. Megi took considerable time to intensify, whereas the model simulated pressure and wind speed intensity are both ahead of the observed values until after 72 hours.

The effect of running no shallow convection follows the trend in the other cyclone cases, where only the G3 case shows sensitivity. Simulated pressure (Fig. 3k) indicates no difference for TD and KF, minimal difference in BMJ, and a large separation beginning after 60 hours for G3 and G3_NS. While there is a large difference in G3 pressure, the same is not seen in the wind speed average (Fig. 3l). This can be caused by changes in the pressure gradient or storm size.

4.2.4 Summary

For the cases, the intensity sensitivity resulting from changing the CP scheme is greater than the sensitivity from initial condition changes. This agrees with the simulated track result. The only case to show sensitivity to initial conditions was Megi for G3 and G3+6. In addition, the use of no shallow convection shows minimal difference to the simulations that used shallow convection, all except the G3 and G3_NS runs.

4.3 Physical mechanisms for sensitivity to cumulus scheme

Based on the examination of cyclone track behaviour, we concentrate our analysis on the differences between the KF and the BMJ simulations, and the G3 and G3_NS simulations. This is because KF and BMJ are physically different CP schemes, being essentially mass-flux and convective adjustment schemes respectively, consistently produced tracks which varied from each other. Furthermore, the track sensitivity between the G3 simulation, where the shallow component of the G3 scheme was switched on, and the G3_NS simulation, where shallow was switched off, was quite marked. Note that the TD simulations are not analysed further because the KF, G3_NS and TD tracks were similar, and with all of them being mass flux schemes, only KF was selected for comparison to BMJ.

4.3.1. Yasi

The KF and BMJ simulations produced considerably different modelling outcomes (Fig. 2). While both simulations had a westward and poleward track similar to observations, the BMJ (solid blue) was displaced much further south-westward than KF (solid red). A similar comparison can be made between G3 (solid green line) and G3_NS (green dashed line) (Fig. 2c).

A comparison of the TC motion and steering vectors for KF (Fig. 4a) and BMJ (Fig. 4b) shows rather different motion between the schemes. Hours 12 – 24 are a crucial period in this study, as during this period KF tracks at 267° (Fig. 4a,ii) while BMJ tracks at 237° (Fig. 4b,ii), thereby leading to a substantial difference in position between the two after 24 hours. Another substantial deviation occurs over hours 36 – 48. At this particular time, KF is tracking at 248° (Fig. 4a,iv), but BMJ is at 227° (Fig. 4b,iv), leading to an even greater separation between the two tracks. For the remainder of the simulation, the two track directions are very similar, so the resulting difference between the two simulations is driven by the differences over hours 12 – 24 and 36 – 48. In addition, if we also consider steering, after 48 hours of simulation (e.g. onward from hour 48 of the simulation), the steering current vector mostly shows less angular difference from the motion vector in KF, which indicates the beta effect is generally less than that in BMJ. The steering current magnitudes are not necessarily larger in BMJ; it is simply that there is a difference in their direction. A greater beta effect in BMJ (a function of differences in the TC motion vectors between KF and BMJ, and the larger storm size in BMJ [not shown]) likely results in greater poleward motion. In this case, for a westward moving storm in the Southern Hemisphere, beta drift typically adds an additional southward component of motion to the steering flow (Holland 1984; Carr and Elsberry 1990).

A similar comparison can be made for the simulation outcome between G3 and G3_NS (green solid and green dashed lines in Fig. 2c). The TC motion and steering vectors (Fig. 4c for G3 and Fig. 4d for G3_NS) show the differences between the two cases. There is a difference in the first 12 hours of simulation, which is negated after 24 hours because the two tracks are then in the same location. A key separation occurs between the hours of 36 –

48 (compare Figs. 4c,iv and 4d,iv), which is the main reason for the subsequent difference in simulated track outcome. At 36 hours, G3 turns to a heading of 239°, while G3_NS turns to a heading of 248°. The result is the G3 simulation moving the TC further south (16.1 °S, 155 °E) and G3_NS further north (15.9 °S, 154.6 °E), respective to their positions at hour 36. Once the two tracks are separated the difference is maintained, with a motion difference of 10° between the two cases over hours 48 – 60 and 60 – 72. The resulting difference in landfall position is driven by these subtle differences. In addition, if steering is considered, we note that the magnitude of the steering current in G3 increases relative to G3_NS over time (e.g. G3 is 0.8 m s^{-1} larger than G3_NS for 60 – 72). An angular difference between the TC motion and steering also develops in G3 that is not seen in G3_NS until hours 72 – 84 (compare Fig. 4c,v-vii with 4d,v-vii). Like BMJ, a greater beta effect in G3 likely results in greater poleward motion compared to G3_NS, but convective effects cannot be ruled out, and will now be examined.

For the purposes of analysing the differences in the simulated track between the cases, we present a table assessing the simulated TC motion against the diagnosed motion derived from the WN-1 PVT analyses, the findings of which are given in Table 6 – 8 as directions in degrees. In order to make a direct comparison, for the specific times analysed we calculate the TC motion over a 6 hour period. We here define "agreement" as cases where there is a small difference between the direction of TC motion and the WN-1 PVT diagnostic. To quantify these descriptions, in terms of the agreement between the WN-1 PVT and the simulated TC motion, if we take a typical storm speed of 15 km/h (4.1 m s^{-1}) and the difference between the WN-1 PVT and the simulated TC motion was 30°, then there is a distance deviation of less than one-half of the actual distance travelled by the storm (note that we used the 6 hour TC motion speed). In such a situation we would quantify the agreement between the WN-1 PVT and simulated TC motion as fair. Good agreement would therefore be any deviation lower than this, and poor agreement anything substantially higher. In terms of whether a storm is strongly steered, we quantitatively define a strongly steered storm as one that has a steering current magnitude above the average distribution of the steering current magnitudes observed in these experiments. For the cases where the directional agreement between the two is not good, other dynamics, such as the convective structure, are studied to help explain why the directions may not match.

The overall conclusion of Tables 6-8 is that while agreement between the TC track direction and the WN-1 diagnostic is usually good, there are important periods of disagreement. In order to explain the track difference between CP schemes, we choose analysis times where there is a significant track difference. For KF and BMJ, we identified this as between hours 12 – 24 (Fig. 4a,ii and 4b,ii) and 36 – 48 (Fig. 4a,iv and 4b,iv). For G3 and G3_NS this is for hours 36 – 60 (Fig. 4c,iv-v and Fig. 4d,iv-v). We have avoided analysing hours 0 – 12 in each case because the storm structure is still developing. Comparing KF and BMJ, we note the largest track difference between the hours of 12 – 24 occurs during hours 12 – 18, where the difference between the two tracks is 37°. For hours 36 – 48, the largest difference occurs during the 6 hours of 36 – 42, where the difference is 32°. Comparing G3 and G3_NS, for hours 36 – 48, the largest difference occurs in the 6 hour period of hours 36 – 42 and is 13°. For hours 48 – 60, the greater difference occurs during hours 54 – 60 (10°). We analyse these important periods of difference and examine one of the time periods for KF / BMJ, and G3 / G3_NS more closely.

For Yasi, we identify several instances where there is significant disagreement between the simulated TC motion and the WN-1 PVT (Table 6, column 4). The differences between the simulated TC motion and WN-1 PVT for KF are large in every instance. In contrast, the only time BMJ showed moderate disagreement (30°) was during hours 18 – 24. Returning to the key times of track difference between the schemes, during hours 12 – 18, KF showed a PVT direction disagreement of 113° and BMJ only 7° (Table 6; compare Fig. 4a,ii and 4b,ii). For hours 36 – 42, KF showed a disagreement of 60° and BMJ only 17° (Table 6; compare Fig. 4a,iv and 4b,iv). During both these periods, KF was not subjected to any substantial steering, while BMJ was strongly steered. This is supported by the better WN-1 and TC motion agreement in BMJ. As previously stated, in the case of a westward moving storm in the Australian region like Yasi, beta drift adds an additional southward component of motion to the steering flow (Holland 1984; Carr and Elsberry 1990), which would explain the simulated motion vector of the storm shown in Fig. 4b,iv. KF, while partially subjected to the same influence, may be affected more by an evolving convective asymmetry, as the agreement between the TC motion and the diagnosed WN-1 PVT is not as good. This is therefore a possible cause for the track difference between KF and BMJ.

We can test this idea by examining the convection over one of the time periods where there is greater disagreement. For the second period of track deviation between the two cases, over hours 36 – 42, we show a difference of 60° between the WN-1 PVT and the TC motion for the KF run (Fig. 5). We also note the steering current magnitude in KF is 1.3 m s^{-1}, and for BMJ is 4.4 m s^{-1}. The direction of the steering in KF is 112° but for BMJ 230°, only 3° different from the TC motion (227°). The small disagreement between the WN-1 PVT and the TC motion for BMJ (17°) indicates a strongly steered storm. For KF, however, because the steering is weak and because the disagreement is large, we suggest that the convection is ultimately responsible for this poor agreement between the WN-1 PVT and the simulated TC motion and the subsequent difference in the two TC tracks. This is further supported by the TC motion vectors in Fig. 4a,iv and 4b,iv and the two tracks in Fig. 2a (BMJ is further southwest, which indicates a storm undergoing stronger beta drift). If we examine the simulated convection for KF over the 36 – 42 time period (Fig. 6), we note that convective asymmetry is present. The maximum convection is shown to rotate around the storm over time, from hour 36 (Fig. 6a) where there is a region in the south east and north west, to hour 38 (Fig. 6b) where the convection has rotated clockwise. At hour 40 (Fig. 6c) and 42 (Fig. 6d), there is a predominance of convection to the north and west of the storm centre. In theory, this should act to deflect the TC away from the motion (190°) diagnosed by the WN-1 PVT (indicated by the solid arrow in Fig. 5), to the simulated motion of 250° (dashed arrow in Fig. 5). This approximately relates to the clockwise rotation of the convection in KF, particularly over the latter periods of hours 36 – 42. We hypothesise that the TC is deflected by the convection, further to the west away from its PVT-diagnosed course. This deflection is derived due to the fact a TC can propagate left or right of the vertical shear vector via advection of PV by the vortex circulation. Convective asymmetries develop from this interaction, often from vortex tilt and stretching. The convective asymmetry can then deflect the TC.

For the G3 and G3_NS cases, we note that there is greater disagreement between the storm motion and the WN-1 diagnostic for the G3_NS case (Table 6). For instance, during hours 36 – 42, the track direction difference between the G3 and G3_NS cases was only 13° but the WN-1 PVT vs. TC motion disagreement was 14° for G3 and 47° for G3_NS. The steering current magnitude and direction in G3 were 5 m s^{-1} and 240°, only 2° different from the TC motion (238°). G3_NS had a steering magnitude and direction of 4.8 m s^{-1} at 247° (the TC motion was 251°). Likewise, over hours 54 – 60, when the track direction difference was only 10°, the WN-1 PVT v TC motion disagreement was 19° and 72° for G3 and G3_NS respectively. Here, the steering for G3 was 5.7 m s^{-1} at 224° (the TC motion was 237°), while in comparison, G3_NS was 5.1 m s^{-1} at 240° (the TC motion was 247°). Both cases had similar steering current magnitudes, and the angular difference between the TC motion and the steering current direction was insignificant in each case. The larger disagreement between the WN-1 PVT and simulated TC motion in G3_NS might be the result of convective effects.

If we examine the convective field for G3_NS over 36 – 42 (Fig. 7), we note the influence of convection, which is a possible reason for the substantial disagreement between the WN-1 PVT diagnostic and the TC motion. The storm is highly asymmetric and the direction of the asymmetry is rapidly changing. The maximum convection is initially mostly located in the same general direction as the TC motion, with the bulk of convection in the western quadrant of the storm environment, rotating clockwise over time. Here we have another case where the TC motion appears not yet to have fully adjusted to developing asymmetries in the convective patterns, resulting in a large disagreement between the actual and PVT-diagnosed storm motions, as suggested by Chan et al. (2002).

In summary, for Yasi we have a clear and systematic response in the convection for the KF and G3_NS cases. These two cases had the largest disagreement between the WN-1 PVT and the simulated TC motion, accompanied by a deflection of the TC track and a subsequent westward moving storm. In contrast, for the BMJ and G3 cases, where there was less disagreement, these storms also showed stronger steering. This resulted in the TC track following the diagnosed motion from the WN-1 PVT more closely, but also meant the additional southward component in the TC motion, driven by beta drift, caused these tracks to move further southward and poleward. We hypothesise that this led to separation from the KF and G3_NS tracks.

4.3.2. Rita

Simulations of hurricane Rita also produced a number of outcomes, particularly during the latter stages of the life cycle. The BMJ+6 (dashed blue in Fig. 2d) and G3+6 (dashed green in Fig. 2d) simulations produced more northward curvature and, being in the Northern Hemisphere, more subsequent poleward motion than the KF+6 (dashed red in Fig. 2d) and G3+6_NS (dashed green in Fig. 2f) simulations. This is the same systematic behaviour that the Yasi simulations displayed. There was more sensitivity to initial conditions than the Yasi simulations showed, but for this storm the sensitivity of track to the choice of CP scheme was still greater than the sensitivity to the initial conditions. Note we have analysed the +6 simulations here as these gave superior track and intensity results (except for TD+6, but this case is not analysed here).

Key periods of difference in track direction include hours 24-36 (compare Fig. 8a,iii and 8b,iii) and hours 36-48 (Fig. 8a,iv and 8b,iv) and afterwards. The resulting subsequent difference in tracks between KF+6 and BMJ+6 is largely due to the differences over these key periods (24 – 48 hours). With regard to the steering, we note that BMJ+6 is subjected to a stronger and more poleward steering current than KF+6 over the latter stages of the simulation (compare the magnitude of the blue coloured vectors in Fig. 8a and 8b), which sufficiently explains the poleward drift of BMJ+6.

A similar comparison can be made for the G3+6 and G3+6_NS simulations (Fig. 8c and 8d). As was the case in Yasi, the G3+6 and G3+6_NS TC tracks are not separated by as large a distance as seen in KF+6 and BMJ+6, but rather result from gradual separation occurring after the first 12 hours. Key periods of differences in track direction include hours 24-36 (compare Fig. 8c,iii and 8d,iii) and hours 60-72 (Fig. 8c,vi and 8d,vi). In addition, the G3+6 NS run does not appear to be as strongly steered as the G3+6 run.

In order to explain the difference in simulation outcome, we now explore the WN-1 PVT diagnostic for the key periods of difference, for both cases. Similarly to the Yasi analysis, for the purposes of examining track sensitivity, we use a 6 hour WN-1 PVT (Table 7). We have not analysed G3+6 and G3+6_NS for hours 24 – 30, 36 – 42, and 66 – 72 because the track difference for these times is not substantial. Unlike Yasi, there are no instances where the disagreement between the simulated TC motion and the diagnosed motion from the WN-1 PVT is large. This means there must be another cause for the difference in TC track between each case. This is because if an evolving convective asymmetry were the cause, then we would expect one case to have large disagreements in the simulated versus diagnosed motion, compared to the other case. For example, for hours 36 – 42, where the track difference between KF+6 and BMJ+6 was 25°, the disagreement between the simulated and diagnosed TC motion was only 9° for KF+6 and 8° for BMJ+6, clearly indicating that the evolution of convective asymmetry is not the cause here. Where there is no disagreement, as here, then a component of the WN-1 PVT equation (e.g. steering current, beta drift or diabatic heating) must be responsible for the different simulated TC track outcome in this case. We examine the steering current for 36 – 42 hours. If steering were responsible for the track difference between these two cases, then we should see some difference in the KF+6 and BMJ+6 steering. In KF+6, the steering current direction is 265° with a magnitude of 1.62 m s^{-1}. For BMJ+6, the direction is 264° at 1.6 m s^{-1}. Both these values are similar to the 36 – 48 hour value for each case (see Fig. 8a,iv and 8b,iv). There is no significant difference in the steering between these two cases. Given this similarity, the difference in track may be due to differences in beta drift or diabatic heating. Here we note that the diabatic heating field, which incorporates stratiform heating, is a more complete representation of the possible effects on storm motion than convective heating alone (e.g. Wang and Wu 2004). The WN-1 diagnostic will include convective effects if they are correctly simulated, such that if the agreement between the TC motion and the WN-1 PVT is good, then the model is capturing the diabatic heating process well. If not, then changes in motion might be related to the diabatic heating field. This is particularly relevant if the steering and beta drift cannot explain the track difference between two cases.

For beta drift to be responsible, the steering current direction would need to be in such a direction to match the expected motion of a storm undergoing beta drift. Based on Chan et al. (2010, see their Fig. 1), in the case of KF+6, a westward moving storm during this time (279°), the beta drift would be to the west (270°). The steering current vector would therefore need to be to the right of the TC motion vector here, but this is not the case (6 hour motion vectors not shown, but similar to that in Fig. 8a,iv). We show this concept in a schematic diagram (Fig. 9a). Fig. 9 shows schematically the contrasting relationship between TC motion, steering currents and the beta effect. In Fig. 9a, a storm travelling towards the northwest in the Northern Hemisphere would experience a beta drift towards the west. In contrast, Fig. 9b shows that a storm moving more to the west would experience a beta drift roughly in the same direction. Therefore, we conclude that the TC motion is not consistent with the combined steering and beta effect, as the beta effect alone does not explain the motion of KF+6. For BMJ+6, a westward moving storm (254°), the beta effect is also to the west (270°). There is likely an effect in BMJ+6 of convective processes as represented here by diabatic heating (Fig. 9b). This is because, unlike in Fig. 9a, where the beta effect alone does not explain the motion of KF+6, in Fig. 9b the beta effect is consistent with the steering current, so that other sources likely contribute to the deflection of the TC track. We examine the extent to which diabatic heating can explain the deflection of the track in the BMJ+6 case. The WN-1 diabatic heating at 42 hours shows quite contrasting fields for KF+6 (Fig. 10a) and BMJ+6 (Fig. 10b). The diabatic heating maximum for BMJ+6 is consistent with the TC motion for this time because the location of the maximum heating matches that of the simulated TC motion direction, but in KF+6, the heating maximum is in the opposite direction to the motion. This indicates there are diabatic heating effects in KF+6 that are contributing to the track difference in some way, but are not necessarily identifiable through diabatic heating asymmetry, as the simulated TC motion and the WN-1 PVT were in good agreement.

We find a similar result for hours 42 – 48, where the track difference between KF+6 and BMJ+6 is 18°, but the WN-1 PVT comparison to the TC motion indicates good agreement in both cases (1° difference for KF+6, 17° for BMJ+6). The steering current for this time period is 259° at 1.4 m s^{-1} in KF+6, compared to 255° at 1.3 m s^{-1} in BMJ+6. The two are similar, indicating steering is not likely responsible for the track difference. In neither case is the motion consistent with the steering current direction as modified by the expected beta effect (not shown), implying that a difference in diabatic heating is one possible cause for the track difference.

With regard to the G3+6 and G3+6_NS cases, for hours 30 – 36, where the track difference was 17°, the WN-1 PVT comparison to the TC motion yielded a disagreement of only 15° for G3+6 and 14° for G3+6_NS (Table 7), showing that the agreement is good. In both cases the TC is deflected slightly to the right of the WN-1 PVT diagnostic (not shown). The steering current for G3+6 at this time is 261° at 2.2 m s^{-1}, for G3+6_NS it is 254° at 2.5 m s^{-1}. It is plausible that a steering direction difference of 7° may be enough to explain the difference in the two TC tracks over this time, but this seems unlikely. For these westward moving storms, the direction of the beta drift would also be westward. In both cases, the motion is not consistent with the steering current direction as modified by the expected beta effect (not shown), so we have a similar situation to the KF and BMJ cases, where diabatic heating effects may explain the track difference. Rates of heating in G3+6 (Fig. 10c) are shown to be greater than G3+6_NS (Fig. 10d) for this time period. The location of the maximum is different also. In G3+6 this tends to oppose the direction of motion, and in G3+6_NS this is in the same direction of motion. G3+6 is tracking further to the north of G3+6_NS, possibly because the diabatic heating maximum in the G3+6 run is to the north.

In summary, Rita is a case where the agreement between the WN-1 PVT and the simulated TC motion was good. Unlike Yasi, where the time evolution of the convective effects in two of the CP schemes, as shown through poor agreement with the WN-1 PVT, was a possible cause of the track difference between cases, we do not find this for Rita. We showed that, in the case of KF+6/BMJ+6, the track difference is either the result of beta drift or diabatic heating differences in BMJ+6 (hours 36 – 42), or diabatic heating differences alone (hours 42 – 48). In the case of G3+6/G3_NS+6, the track difference may be the result of diabatic heating differences over 30 – 36 hours and steering current differences over 60 – 66 hours.

4.3.3. Megi

As the simulated tracks in Fig. 2 indicated, super typhoon Megi proved to have the most variation among simulations, that is, there was less consistent grouping between some simulations (e.g. KF and TD and G3_NS tracks together, and BMJ and G3 tracks together, as seen in Yasi and Rita). There was still a difference, however, between the G3 and G3_NS and the BMJ and KF cases. In fact, G3_NS and G3 (green coloured tracks in Fig. 2i) varied the most of any pairing across the three cyclone cases.

In the case of the TC motion for KF (Fig. 11a) and BMJ (Fig. 11b), differences in the motion in the early stages contribute to the difference in the tracks later. In addition, the looping of the BMJ track between hours 72 – 96 is reflected in the TC motion vectors (Fig. 11b,vii-viii). During the first 12 hours, KF is tracking at 180° and BMJ at 281°. The subsequent track difference over hours 12 – 36 is an artefact of the initial displacement. Note that it is possible for a TC to move faster than the steering current, usually a sign of a dominant beta effect (e.g. Carr and Elsberry 1997). The period of 36 – 48 hours is a key period of difference between the cases: KF tracks at 297° and BMJ at 317°, a 20° difference. The following 12 hours (48 – 60) proves to be another period of difference. KF tracks at 296° and BMJ at 306°. Both cases show a rapid increase in TC speed, so that BMJ is now at a similar longitude to KF but due to the track difference, much further north (KF at 16.1 °N, 133.7 °E; BMJ at 16.9 °N, 134 °E). During the final stages prior to landfall, KF shifts course to 254° over hours 96 – 108, taking it further south of BMJ. KF continues to track similarly in this direction over hours 108 – 120 to make landfall further south of BMJ, which due to the

96 – 108 motion has resulted in landfall much further north and some 12 hours after KF.

Like the Yasi and Rita cases, for Megi there was sensitivity to the use of shallow convection in the G3 scheme (Fig. 2i). G3 does not make landfall and tracks well to the north of G3_NS, which follows a course similar to the best track (black solid line in Fig 2i). The result for this parameterisation shows a systematic sensitivity to the shallow convection, as also observed in Yasi and Rita.

The key difference between the two cases occurs over hours 48 – 60 (Fig. 11c,v and 11d,v) when G3 tracks at 284° and G3_NS 295°, for a difference of 11°. At the end of 60 hours, this key difference in TC motion has G3_NS further north of G3. Over hours 72 – 84 (compare Fig. 11c,vii and 11d,vii), G3 shows a northward curvature in its track. This is reflected in the steering vectors, where the storm is now more strongly steered over these latter times (Fig. 11c,vii-x), compared to G3_NS which is not nearly as strongly steered (Fig. 11d,vii-x).

G3_NS makes landfall sometime during the 108 – 120 period, but G3 makes a sudden turn to the north at hour 120. This is illustrated by additional vector plots for hours 120 – 132 and 132 – 144 (Fig. 12). The steering current for 120 – 132 hours is 53° at 3.8 m s^{-1} and this increases in magnitude to 4.8 m s^{-1} with a direction of 54° for hours 132 – 144. Clearly G3 is being strongly steered over this time so that the storm continues to drift north. This result is most likely a function of the storm slowing from hour 60, relative to G3_NS, which increased in speed and translated the TC further west. This would have placed G3 in a different steering environment compared to G3_NS and this slowing of G3, possibly also driven by differences in simulated convection, has led to a different simulated outcome.

We test this hypothesis for both Megi convective comparisons. The results of the WN-1 PVT diagnostic for Megi are shown in Table 8. We analyse the WN-1 PVT for the time periods where the 6 hour TC track difference was large. We have once again calculated the WN-1 PVT as a 6 hour time tendency to minimise the effect of storm movement, so we analyse the key periods of track difference by splitting the 12 hour motion vector into two 6 hour periods. There are also some additional time periods analysed to explore some of the track behaviour noted later in the simulation.

We note that similarly to Rita, the overwhelming majority of the periods analysed show good agreement between the simulated TC motion and the WN-1 PVT diagnosed motion. There is only one case where the agreement is poor (BMJ). This indicates that time evolution of convective asymmetry is a possible cause for track deviation in the KF and BMJ comparison. For hours 42 – 48, the difference between the WN-1 PVT and the TC motion in KF is only 9°, but for BMJ it is 42° (Table 8). This is accompanied by the 28° separation in these tracks as stated. For hours 48 – 54, the disagreement between the WN-1 PVT and TC motion in KF is 13° and for BMJ it is 29°. The diagnostic disagreement therefore decreased from the previous time to 16°, which may be indicative of a decrease in deflection of BMJ. To show that convective effects are a possible reason for the poor agreement in BMJ and subsequent track difference from KF, we show a time series of simulated reflectivity (Fig. 13). There is clearly a bias of convection to the north of the eye and the asymmetry is present across the entire 6 hour period. The TC is likely deflected toward the region of convective asymmetry. Here we see another possible example of an angular shift in the direction of maximum WN-1 PVT occurring before a corresponding change in direction of the storm motion, in this case possibly driven by transient convective effects. This causes the disagreement to decrease with time for the BMJ run.

For the track deviation in G3 and G3_NS, the results indicate the agreement between the WN-1 PVT and the simulated TC motion was good for both cases during the key times of track difference. We hypothesise that the simulated convection in both cases (not shown) is not anomalous enough to cause significant disagreement between the WN-1 PVT and the simulated TC motion, but nevertheless it is different between the two cases, so that a track difference between G3 and G3_NS arises. In order to assess the cause of the track difference, we undertake the same assessment that we performed for Rita. We note that because the convective effects are associated with the diabatic heating, that this component of the PVT diagnostic equation is most likely to be the cause for the track difference rather than the steering or beta effect. With regard to the steering current for hours 48 – 54, for G3 this was 311° at 2.4 m s^{-1} and 299° at 2.4 m s^{-1} for G3_NS, indicating similar steering. An analysis of the beta effect shows that the TC motion is consistent with the steering current direction as modified by the expected beta effect in both cases (not shown). Therefore, in the absence of differences in either of those two components of the PVT diagnostic equation, a difference between the simulations in the diabatic heating is the most likely cause of the track difference. Indeed, we note there are contrasts in the diabatic heating of these storms during this time. The WN-1 diabatic heating at time 54 (Fig. 14) shows the location of the maximum rate of heating aligns with the track direction in each case. In G3 (Fig. 14a), the heating maximum closest to the storm center is southwest and in G3_NS (Fig. 14b) this is north. G3_NS is tracking further north of G3 possibly because its diabatic heating maximum is to the north, whereas G3 tracks further south of G3_NS because the diabatic heating maximum is to the south. This is driven by convective differences and indicates there are convective effects in both cases that are contributing to the track difference, but are not necessarily identifiable in the analysis conducted here.

In summary, Megi is another case where the majority of WN-1 PVT comparisons to the simulated TC track were in good agreement. The BMJ case, was the only case in poor agreement. The simulated track difference between BMJ and KF was largely the result of convective asymmetry in BMJ occurring over hours 42 – 54. For G3 and G3_NS, we showed that the simulated convection in both cases was not anomalous enough to cause significant disagreement between the WN-1 PVT and the simulated TC motion, but was nevertheless different between the two cases. This difference in convection was illustrated through the contrasting fields of the WN-1 diabatic heating for G3 and G3_NS.

5. Summary and conclusions

The objective of this study was to ascertain and attempt to quantify how sensitive tropical cyclone (TC) tracks are to changing the convective parameterization scheme in the WRF model. A diagnostic study of three major hurricanes from different basins was undertaken, using the Kain-Fritsch (KF), Betts-Miller-Janjic (BMJ), Grell-3D (G3) and Tiedtke (TD) convective parameterization (CP) schemes. In order to assess the track differences and explain the physical mechanisms of these differences, we used several diagnostics, including differences in steering currents and a WN-1 potential vorticity tendency diagnostic for TC motion derived by Wu and Wang (2001) and Chan et al. (2002).

The major findings of this study are as follows:

1. The sensitivity of TC track to initial conditions (the initialisation time and model domain size) is less than the sensitivity of TC track to changing the convective parameterizations scheme.

2. The TC track is not particularly sensitive to the specification of shallow convection in the KF, BMJ and TD schemes, but is highly sensitive in the G3 scheme. This is a systematic finding across all three cyclone cases.

3. The G3 simulation consistently performed poorly across all three cyclone cases. The no shallow simulation, G3_NS, was consistently better performing.

4. In general, agreement between the model-simulated track and the WN-1 diagnostic is good, but with important exceptions that are often associated with model-generated

convective asymmetries. Storms that are more strongly steered appear to show better agreement between the TC track and the WN-1 diagnostic.

We have shown greater sensitivity to TC track from changing the CP scheme than from initial condition changes. The contribution of initial condition error to model forecast error is a topic of ongoing research, with sophisticated attempts to improve model initialisation for TC forecasting (e.g. ensemble Kalman filter, data assimilation etc. Kalnay 2003). Here we used WRF in its standard configuration with no additional initialisation techniques such as bogussing or data assimilation. We were able to reproduce both the TC track and intensity to a reasonable standard, with minimal TC track error. It is arguable whether there would be significant improvement from the use of more advanced initialisation techniques in these cases, but we might expect some improvement in simulated intensity and TC track. Running the same simulations again with a different initial dataset (e.g. ECMWF analyses) would be useful to assess the sensitivity to the forcing dataset, but it still seems unlikely the sensitivity to initial conditions would be larger than the change from CP. Moreover, the initialisation time chosen to test for initial condition sensitivity was only 6 hours later. While this should be adequate to test initial condition sensitivity, simulations from a different stage of TC life cycle (e.g. the intensification or mature stage) might show sensitivity to initial conditions. This would require a good assimilation / bogussing scheme and such tests are beyond the scope of this study, but recommended for future work.

Errors in TC track forecasts tend to be related to wind errors associated with the simulation of the large scale synoptic environment (Carr and Elsberry 2000). TC motion is controlled by the large scale synoptic flow (environmental wind) over the tropospheric deep layer, which is driven by the large scale weather systems in the vicinity combined with the beta effect (Holland 1983). Therefore it is important to capture the large scale synoptic environment to help minimise errors in TC motion. We addressed this issue by running a sufficiently large coarse domain (5076 × 3888 km of 12 km grid spacing) and by using the 1 × 1 degree NCEP FNL data (i.e. a final analysis dataset comprising 10 % more observations than GFS; Environmental Modeling Center, 2003). As a by-product of changing the model domain size, we were then able to assess the sensitivity to initialisation of the large scale environment and its effect on the TC track. Since the sensitivity in TC track from model domain size changes was less than that of changing the CP scheme, we can conclude there is greater sensitivity in TC motion to changing the CP scheme. This is likely a function of each CP representing the initial environment slightly differently, but also a result of the dominating effect of the CP scheme on TC structure through its representation of convection.

There has been limited work devoted to the assessment of TC track sensitivity to CP scheme, and perhaps more importantly, the studies which have done so are varied in their methodological approach. Recent work (e.g. Sun et al. 2013; Sun et al. 2014a,b; Sun et al. 2015) has drawn conclusions about schemes specific to a particular storm event and has not attempted to reach systematic conclusions about CP performance. As an example of the varied nature of outcomes in this field, Sun et al. (2013) found that G3 presented better simulation results than KF and BMJ for storm intensity and structure. In the present study, we showed that G3 often produced the poorest representation of structure when compared against observations from each of the cases (e.g. an eye that was too large, an excessively large storm size).

The methodological approach used here, where the Chan et al. (2002) WN-1 PVT diagnostic was applied, is also to our knowledge the first instance where it has been applied to study TC track sensitivity to CP. Chan et al. (2002) states this method is useful for evaluating numerical weather prediction model performance, and whether the maximum cyclonic PVT can be captured by the model and whether this aligns with the TC motion. We showed that the WN1-PVT diagnostic is generally a good indicator of TC motion, but when we assessed the WN-1 PVT diagnosed motion against the simulated TC motion for each individual CP scheme, we showed some instances of disagreement. The Rita and Megi hurricane case studies generally showed good agreement between the WN-1 PVT and the simulated TC motion, where Yasi showed large differences for two of the CPs. the likely result of simulated convective asymmetry.

With regard to implications for modelling of TCs, we can make some general statements about what these findings mean from a modelling perspective. In order to make a general statement about CP performance, including which scheme is best at representing the large scale environment and convective processes in the TC vortex, many more cases would be required. What we have shown here, however, is that there is a systematic sensitivity of TC track to CP scheme that we established across three cases from different basins. In particular, the G3 scheme is highly sensitive to shallow convection, whereas the KF, TD and BMJ schemes are not. More accurate TC track and intensity representation was achieved with the no shallow convection configuration of G3. The WRF model successfully captures the cyclonic maximum of the WN-1 PVT and this diagnostic can be applied to successfully diagnose dynamical differences in TC motion as simulated by parameterisation schemes. This technique could also be applied to test sensitivity to other parameterisations (e.g. microphysics).

Acknowledgements

This research was undertaken with the assistance of resources from the National Computational Infrastructure (NCI), which is supported by the Australian Government. Further funding was provided by the Edward and Isobel Kidson Scholarship through Universities New Zealand and AMP New Zealand, and the Australian Postgraduate Award. The authors would also like to thank Jimy Dudhia for scientific advice and Cindy Bruyère for comments on an earlier draft.

References

Arakawa A (2004) The Cumulus Parameterisation Problem: Past, present, and future. J. Climate. 17:2493–2525.

Arakawa A, and Schubert WH (1974) Interaction of a cumulus cloud ensemble with the large-scale environment, Part I. J. Atmos. Sci. 31:674–701.

Bassill NP (2014) Accuracy of early GFS and ECMWF Sandy (2012) track forecasts: Evidence for a dependence on cumulus parameterization. Geophys. Res. Lett. 41:3274–3281.

Betts AK (1986) A new convective adjustment scheme. Part I: Observational and theoretical basis. Quart. J. Roy. Meteor. Soc. 112:677–691.

Betts AK and Miller MJ (1986) A new convective adjustment scheme. Part II: Single column tests using GATE wave, BOMEX, ATEX, and Arctic air-mass data sets. Quart. J. Roy. Meteor. Soc. 112:693–709.

Bougeault P (1985) A simple parameterization of the large-scale effects of cumulus convection. Mon. Wea. Rev. 113:2108–2121.

Bretherton CS, McCaa JR, and Grenier H (2004) A new parameterization for shallow cumulus convection and its application to marine subtropical cloud-topped boundary layers. Part I: Description and 1D results. Mon. Wea. Rev. 132:864–882.

Brisbane Times, cited 2015: Yasi bill revealed: $800 million in damages. [Available online at http://www.brisbanetimes.com.au/queensland/yasi-bill-revealed-800-million-in-damages-20110216-1avvu.html]

Cao Y, Fovell RG, and Corbosiero KL (2011) Tropical cyclone track and structure sensitivity to initialization in idealised simulations: a preliminary study. Terr. Atmos. Ocean. Sci. 22:559– 578.

Carr LE III, and Elsberry RL (1990) Observational evidence for prediction of tropical cyclone propagation relative to environmental steering. J. Atmos. Sci. 47:542–46.

Carr, LE III, Elsberry R (1997) Models of tropical cyclone wind distribution and beta-effect propagation for application to tropical cyclone track forecasting. Mon. Wea. Rev., 125: 3190–3209.

Cha D-H, Wang Y (2013) A dynamical initialization scheme for real-time forecasts of tropical cyclones using the WRF model. Mon. Wea. Rev. 141:964–986.

Chan JCL, Ko FM, and Lei YM (2002) Relationship between potential vorticity tendency and tropical cyclone motion. J. Atmos. Sci. 59:1317–1336.

Chan JCL, and Kepert JD (Eds.) (2010) Global Perspectives on Tropical Cyclones – From Science to Mitigation. World Scientific Publishing, 444 pp.

Chan JC, and Williams RT (1987) Analytical and numerical studies of the beta-effect in tropical cyclone motion. Part I: Zero mean flow. J. Atmos. Sci. 44:1257-1265.

de Szoeke, SP, Wang Y, Xie S-P, and Miyama T (2006) The effect of shallow convection on the eastern Pacific climate in a coupled model. Geophys. Res. Lett. 33, L17713. doi:10.1029/2006GL026715.

Davis C, Wang W, Chen S, Chen Y, Corbosiero K, DeMaria M, Dudhia J, Holland G, Klemp J, Michalakes J, Reeves H, Rotunno R, Snyder C, and Xiao Q (2008) Prediction of Landfalling Hurricanes with the Advanced Hurricane WRF Model. Mon. Wea. Rev. 136:1990–2005.

Dengler K, and Reeder MJ (1997) The effects of convection and baroclinicity on the motion of tropical-cyclone-like vortices. Quart. J. Roy. Meteor. Soc. 123:699–725.

Dudhia J (1989) Numerical study of convection observed during the winter monsoon experiment using a mesoscale two-dimensional model. J. Atmos. Sci. 46:3077–3107.

Emanuel KA (1989) The finite-amplitude nature of tropical cyclogenesis. J. Atmos. Sci. 46:3431–3456

Emanuel KA (1991) A scheme for representing cumulus convection in large-scale models. J. Atmos. Sci. 48:2313–2329.

Environmental Modelling Center (2003) The GFS atmospheric model. NCEP Office Note 442, Global Climate and Weather Modeling Branch, EMC, Camp Springs, Maryland.

Fovell RG, Corbosiero KL, and Kuo H-C (2009) Cloud microphysics impact on hurricane track as revealed in idealized experiments. J. Atmos. Sci. 66:1764–1778.

Frank WM (1983) The cumulus parameterisation problem. Mon. Wea. Rev. 111:1859-1871.

Frank WM, and Cohen C (1987) Simulation of tropical convective systems. Part I: A cumulus parameterization. J. Atmos. Sci. 44:3787–3799.

Fritsch JM, and Chappell CF (1980) Numerical prediction of convectively driven mesoscale pressure systems. Part I: Convective parameterisation. J. Atmos. Sci. 37:1722–1733.

Gregory D, and Rowntree PR (1990) A mass flux convection scheme with representation of cloud ensemble characteristics and stability-dependent closure. Mon. Wea. Rev. 118:1483–1506.

Grell GA (1993) Prognostic evaluation of assumptions used by cumulus parameterisation. Mon. Wea. Rev. 121:764–787.

Grell GA, and Devenyi D (2002) A generalised approach to parameterising convection combining ensemble and data assimilation techniques. Geophys. Res. Lett., 29 doi:10.1029/2002GL015311.

Han J, and Pan H-L (2011) Revision of convection and vertical diffusion schemes in the NCEP global forecast system. Wea. Forecasting. 26:520–533.

Hill KA, and Lackmann GM (2009) Analysis of idealized tropical cyclone simulations using the Weather Research and Forecasting Model: Sensitivity to turbulence parameterization and grid spacing. Mon. Wea. Rev. 137:745–765.

Holland GJ (1983) Tropical cyclone motion: Environmental interaction plus a beta effect. J. Atmos. Sci. 40:328-342.

Holland GJ (1984) Tropical cyclone motion: a comparison of theory and observation. J. Atmos. Sci. 41:68–75

Janjic ZI (1990) The step-mountain coordinate: physical package. Mon. Wea. Rev. 118:1429–1443.

Janjic ZI (1994) The step-mountain coordinate model: Further developments of the convection, viscous sub-layer, and turbulence closure schemes. Mon. Wea. Rev. 122:927–945.

Janjic ZI (1996) The surface layer in the NCEP Eta Model. 11th Conf. on Numerical Weather Prediction, Norfolk, VA, 19–23 August; Amer. Meteor. Soc., Boston, MA, 354–355.

Janjic ZI (2001) Nonsingular Implementation of the Mellor–Yamada Level 2.5 Scheme in the NCEP Mesoscale model. NCEP Office Note, No. 437, 61 pp.

Kain JS (2004) The Kain-Fritsch convective parameterization: An update. J. Appl. Meteor. 43:170–181.

Kain JS, and Fritsch JM (1990) A one-dimensional entraining/detraining plume model and its application in convective parameterization. J. Atmos. Sci. 47:2784–2802.

Kain JS, and Fritsch JM (1993) Convective parameterisation for mesoscale models: The Kain-Fritsch scheme. The Representation of Cumulus Convection in Numerical Models, Meteor. Monogr., No. 46, Amer. Meteor. Soc., 165–170.

Kalnay E (2003) Atmospheric modeling, data assimilation, and predictability, Cambridge University Press, Cambridge, 341pp.

Kieu CQ, Truong NM, Mai HT, and Ngo-Duc T (2012) Sensitivity of the track and intensity forecasts of typhoon Megi (2010) to satellite-derived atmospheric motion vectors with the ensemble kalman filter. J. Atmos. Oceanic Technol. 29:1794–1810.

Knabb RD, Brown DP, and Rhome JR (2006) Hurricane Rita tropical cyclone report. National Hurricane Centre Report. Available at: http://www.nhc.noaa.gov/pdf/TCR-AL182005_Rita.pdf

Krishnamurti TN, Han W, and Oosterhof D (1998) Sensitivity of hurricane intensity forecasts to physical initialization. Met. Atmos. Phys. 65:171–181.

Kumar A, Done J, and Dudhia J (2011) Simulations of cyclone Sidr in the Bay of Bengal with a high-resolution model: sensitivity to large-scale boundary forcing. Meteor. Atmos. Phys. 114:123–137.

Kuo HL (1974) Further studies of the parameterization of the influence of cumulus convection on large-scale flow. J. Atmos. Sci. 31:1232–1240.

Li X, and Pu Z (2009) Sensitivity of numerical simulations of the early rapid intensification of hurricane Emily to cumulus parameterization schemes in different model horizontal resolutions. J. Meteor. Soc. Japan. 87:403–421.

Mellor GL, and Yamada T (1982) Development of a turbulence closure model for geophysical fluid problems. Rev. Geophys. Sp. Phys. 20:851–875.

Mlawer EJ, Taubman SJ, Brown PD, Iacono MJ, and Clough SA (1997) Radiative transfer for inhomogeneous atmosphere: RRTM, a validated correlated-k model for the longwave. J. Geophys. Res. 102 (D14):16663–16682.

Molinari J, and Dudek M (1992) The parameterisation of convection in numerical models: A critical review. Mon. Wea. Rev. 120:326–344.

Nasrollahi N, AghaKouchak A, Li J, Gao X, Hsu K, and Sorooshian S (2012) Assessing the impacts of different WRF precipitation physics in hurricane simulations. Wea. Forecasting. 27:1003–1016.

National Centers for Environmental Prediction/National Weather Service/NOAA/U.S. Department of Commerce (2000) NCEP FNL Operational Model global tropospheric analyses, continuing from July 1999. Research Data Archive at the National Center for Atmospheric Research, Computational and Information Systems Laboratory, Boulder, CO.

[Available online at http://dx.doi.org/10.5065/D6M043C6.].

National Disaster Risk Reduction and Management Council, 2010: SitRep No. 12 Effects of Typhoon Megi. [Available online at: http://reliefweb.int/sites/reliefweb.int/files/resources/3B64B52B1B6A5457492577C3001AC81B-Full_Report.pdf].

Ooyama KV (1971) A theory on parameterization of cumulus convection. J. Meteor. Soc. Japan. 49:744–756.

O'Shay AJ, and Krishnamurti TN (2004) An examination of a model's components during tropical cyclone recurvature. Mon. Wea. Rev. 132:1143–1166.

Prater BE, and Evans JL (2002) Sensitivity of modelled tropical cyclone track and structure of hurricane Irene (1999) to the convective parameterisation scheme. Meteor. Atmos. Phys. 80:103–115.

Reuters, cited 2015: Cyclone Yasi to cost insurers AUS $3.5 bln – forecaster. [Available online at http://www.reuters.com/article/2011/02/03/insured-losses-yasi-idUSLDE7121NR20110203]

Rogers E, Black T, Ferrier B, Lin Y, Parrish D, and DiMego G (2001) Changes to the NCEP Meso Eta Analysis and Forecast System: Increase in resolution, new cloud microphysics, modified precipitation assimilation, modified 3DVAR analysis. NWS Technical Procedures Bulletin 488, NOAA/NWS.

Rosier MJ, and Miller DK (2005) Sensitivity of Hurricane Charley simulations to changes in WRF model. Extended abstract, 21st Conf. on Weather Analysis and Forecasting/17th Conf. on Numerical Weather Prediction, Washington, DC, Amer. Meteor. Soc., P1.33. [Available online at: https://ams.confex.com/ams/WAFNWP34BC/techprogram/paper_94821.htm]

Skamarock, WC, Wang W, Barker D, Gill D, Klemp J, and Powers GJ (2008) A description of the Advanced Research WRF Version 3.1. NCAR Technical Note–468+STR.

Srinivas CV, Venkatesan R, Bhaskar Rao DV, and Prasad DH (2007) Numerical Simulation of Andhra Severe Cyclone (2003): Model Sensitivity to the Boundary Layer and Convection Parameterization. Pure Appl. Geophys. 164:1465–1487.

Stensrud DJ (2007) Parameterisation schemes: Keys to understanding numerical models, Cambridge University Press, Cambridge, 459pp.

Sun Y, Lan Y, Zhong Z, Hu Y, and Ha Y (2013) Dependence of model convergence on horizontal resolution and convective parameterisation in simulations of a tropical cyclone at greyzone resolutions. J. Geophys. Res. 118:7715–7732.

Sun Y, Zhong Z, Lu W, and Hu Y (2014a) Why are tropical cyclone tracks over the western North Pacific sensitive to the cumulus parameterisation scheme in regional climate modelling? A case study for Megi (2010). Mon. Wea. Rev. 142:1240–1249.

Sun Y, Yi L, Zhong Z, and Ha Y (2014b) Performance of a new convective parameterisation scheme on model convergence in simulations of a tropical cyclone at grey-zone resolutions. J. Atmos. Sci. 71:2078– 2088.

Sun Y, Zhong Z, Dong H, Shi J, and Hu Y (2015) Sensitivity of tropical cyclone track simulation over the Western North Pacific to different heating/drying rates in the Betts-Miller-Janjic Scheme. Mon. Wea. Rev. doi:10.1175/MWR-D-14-00340.1, in press.

Tiedtke M (1989) A comprehensive mass flux scheme for cumulus parameterization in large-scale models. Mon. Wea. Rev. 117:1779–1800.

Torn RD, and Davis CA (2012) The Influence of shallow convection on tropical cyclone track forecasts. Mon. Wea. Rev. 140:2188–2197.

Wang Y, Xie S-P, Hu, H-M, and Wang B (2004a) Regional model simulations of marine boundary layer clouds over the southeast Pacific off South America. Part I: Control experiment. Mon. Wea. Rev. 132:274–296.

Wang Y, Xu H, and Xie S-P (2004b) Regional model simulations of marine boundary layer clouds over the southeast Pacific off South America. Part II: Sensitivity experiments. Mon. Wea. Rev. 132:2650–2668.

Wang, Y, and Wu CC (2004). Current understanding of tropical cyclone structure and intensity changes–a review. Met. Atmos. Phys. 87: 257-278.

Weisman ML, Skamarock WC, and Klemp JB (1997) The resolution dependence of explicitly modeled convective systems. Mon. Wea. Rev. 125:527–548.

Wu CC, and Emanuel KA (1993) Interaction of a baroclinic vortex with background shear: Application to hurricane movement. J. Atmos. Sci. 50:62–76.

Wu CC, and Wang B (2000) A potential vorticity tendency diagnostic approach for tropical cyclone motion. Mon. Wea. Rev. 128:1899–1911.

Wu CC, and Wang B (2001) Effects of convective heating on movement and vertical coupling of tropical cyclones: A numerical study. J. Atmos. Sci. 58:3639–3649.

Zhang C, Wang Y, and Hamilton K (2011) Improved representation of boundary layer clouds over the Southeast Pacific in ARW-WRF using a modified Tiedtke cumulus parameterization scheme. Mon. Wea. Rev. 139:3489–3513.

Zhu H, and Smith RK (2002) The importance of three physical processes in a minimal three-dimensional tropical cyclone model. J. Atmos. Sci. 59:1825–1840.

Zhu H, Smith RK, and Ulrich W (2001) A minimal three-dimensional tropical cyclone model. J. Atmos. Sci. 58**:**1924–1944.

List of Tables

List of Figures

Fig. 1 The domain configurations for the (a) Yasi, (b) Rita, and (c) Megi cases. Domains 2 and 3 are moving nests. The resolution is 12, 4 and 1.33 km respectively for each domain. The number of grid points were 423 x 324, 201 x 201, 240 x 240 for each domain

Fig. 2 Tracks of the CP simulations for each case study for (a) Yasi 00Z (solid) and +06Z (dashed), (b) Yasi 00Z (solid) and DOM2 (dashed), (c) Yasi 00Z (solid) and NS (dashed), (d) – (f) Rita, and (g) – (i) Megi. The observed track is the black line. The black dots represent the track position at 12 hourly intervals. The KF cases are in red, the BMJ cases are in blue, the G3 cases in green and TD in yellow

Fig. 3 Comparison of the trend in simulated pressure (hPa) and six hour moving average of wind speed (knots), for (a – d) Yasi, (e – h) Rita, and (i – l) Megi. Panel (a) pressure, and (b) wind, compare the Yasi 00Z and +06Z simulations, and panel (c) and (d) the Yasi 00Z and NS simulations. For Rita, (e – f) 00Z and +06Z simulations, and (g – h) +06Z and +6_NS simulations. For Megi, (i – j) 00Z and +06Z simulations, and (k – l) 00Z and NS simulations. The ibTracs observed data is given by the black dots

Fig. 4 TC motion and steering current vectors (in m s^{-1}) for the Yasi simulation, for (a) KF, (b) BMJ, (c) G3, and (d) G3_NS. Each panel shows the vectors at 12-hr intervals, for (i) 0 – 12 hours, (ii) 12 – 24 hours, (iii) 24 – 36 hours, (iv) 36 – 48 hours, (v) 48 – 60 hours, (vi) 60 – 72 hours, and (vii) 72 – 84 hours

Fig. 5 WN-1 PV tendency (in PVU) for KF over simulation hours 36 – 42, for the Yasi case. The solid arrow indicates the diagnosed motion from the WN-1 PV tendency, while the dashed line is the simulated TC motion. Note: this is a southern hemisphere case, and as such blue indicates the cyclonic PV. The output is from domain 1 with a grid spacing of 12 km, but has been coordinate transformed to a new 300 x 300 grid to account for storm movement over 6 hours. 1 PVU = 1.0×10^{-6} m^2 s^{-1} K kg^{-1}

Fig. 6 Simulated radar reflectivity of Yasi for the KF case at (a) 06Z 01 February 2011 at 36 hours of simulation, (b) 08Z at 38 hours, (c) 10Z at 40 hours, and (d) 12Z at 42 hours

Fig. 7 The same as Fig. 6 for the G3_NS case at (a) 06Z 01 February 2011 at 36 hours, (b) 08Z at 38 hours, (c) 10Z at 40 hours, and (d) 12Z at 42 hours

Fig. 8 TC motion and steering current vectors (in m s^{-1}) for the Rita simulation, for (a) KF+6, (b) BMJ+6, (c) G3+6, and (d) G3+6_NS. Each panel shows the vectors at 12-hr intervals for, (i) 0 – 12 hours, (ii) 12 – 24 hours, (iii) 24 – 36 hours, (iv) 36 – 48 hours, (v) 48 – 60 hours, (vi) 60 – 72 hours, (vii) 72 – 84 hours, (viii) 84 – 96 hours, (ix) 96 – 108 hours, and (x) 108 – 120 hours (except for KF+6)

Fig. 9 Schematic diagram showing the TC motion (red line labelled 'TC'), actual steering (solid blue labelled 'S') and beta effect (solid black line labelled 'B') for (a) KF+6 36 – 42, and (b) BMJ+6 36 – 42. In (a), for the tropical cyclone track to be consistent with the steering and the beta effect, the steering current would have to be in the direction of the blue dashed line, with the black dashed line then being in the same direction as the beta effect. In (b), the TC motion is consistent with the steering and the beta effect as the steering is in the same direction as the beta effect. See the text for an explanation

Fig. 10 WN-1 diabatic heating (Pa K s^{-1}) for Rita for (a) KF+6 at 42 hours, (b) BMJ+6 at 42 hours, (c) G3+6 at 36 hours, and (d) G3+6_NS at 36 hours

Fig. 11 TC motion and steering current vectors (in m s^{-1}) for the Megi simulation, for (a) KF, (b) BMJ, (c) G3, and (d) G3_NS. Each panel shows the vectors at 12-hr intervals, for (i) 0 – 12 hours, (ii) 12 – 24 hours, (iii) 24 – 36 hours, (iv) 36 – 48 hours, (v) 48 – 60 hours, (vi) 60 – 72 hours, (vii) 72 – 84 hours, (viii) 84 – 96 hours, (ix) 96 – 108 hours, and (x) 108 – 120 hours

Fig. 12 TC motion and steering current vectors (in m s^{-1}) for 12-hr intervals for the Megi G3 simulation, (a) 120 – 132 hours, and (b) 132 – 144 hours

Fig. 13 Simulated radar reflectivity of Megi for the BMJ case at (a) 06Z 15 at 42 hours, (b) 08Z at 44 hours, (c) 10Z at 46 hours, and (d) 12Z at 48 hours

Fig. 14 The same as Fig. 10 for Megi at 54 hours for (a) G3, and (b) G3_NS

Table 1 Summary of CP schemes used in this study

Scheme	Type of scheme	Cloud detrainment	Closure	Comments	Shallow convection design
BMJ	Convective Adjustment	N	Sounding adjustment	Based on pre-defined reference profiles. Deep convection profiles depend on cloud efficiency.	Shallow convection is a process operating between a buoyant layer and an inversion aloft. The shallow scheme is used if cloud depth < 200 hPa, or if the precipitation rate is negative. The cloud base is the same as for the deep scheme, but the cloud top is defined as the layer that has the fastest decrease in RH.
KF	Mass-flux	Y	CAPE removal	A cloud model based on updrafts and downdrafts.	Activated when all of the criteria for deep convection are satisfied *except* that the cloud model yields an updraft more shallow than the minimum cloud depth (2 km). Precipitation occurs in any shallow cloud deeper than 50 hPa. If an updraft has already been classified as shallow, any precipitation that is generated by the scheme is fed back to resolved scales as an additional moisture source. Closure is based on TKE.

Scheme	Type of scheme	Cloud detrainment	Closure	Comments	Shallow convection design
G3	Ensemble scheme (Mass-flux approach)	Y	Various e.g. CAPE, moisture convergence.	Based on Grell- Devenyi (Grell and Devenyi 2002) scheme. Allows subsidence spreading over neighbouring grid cells.	The fractional area coverage of convective updrafts is first defined. This fractional area is related to the entrainment rate. The entrainment rate determines when the fractional area coverage of convection becomes important. The maximum allowable fractional coverage determines when the CP transforms itself to a shallow convection scheme.
TD	Mass-flux	Y	CAPE	Organised and turbulent entrainment / detrainment.	Shallow convection is parameterized by assuming that the moisture flux through the cloud base is equivalent to the surface moisture flux. Operates in the same way as the deep component using organised turbulent entrainment / detrainment, but with a different rate for shallow convection. Uses a fraction to determine the percentage of the cloud ensemble of shallow convection that penetrates into the inversion layer and detrains there into the environment.

Table 2 Yasi landfall distance differences (in km) for each CP (NS refers to NO_SHALLOW)

Case	*vs. +6*	*vs. DOM2*	*KF vs. other CPs*	*vs. NS CP*	*KF NS vs. other NS CPs*	*KF_DOM2 vs. other DOM2 CPs*	*KF+6 vs. other +6 CPs*
KF	22	73	-	15	-	-	-
BMJ	119	74	329	14	300	184	243
G3	86	61	280	278	21	181	229
TD	10	15	100	37	84	153	84
AVERAGE	59	55	236	86	135	172	185

Table 3 Rita landfall distance differences for each CP

Case	*vs. 00Z*	*vs. DOM2*	*KF+6 vs. other +6 CPs*	*vs. +6NS CP*	*KF+6 NS vs. other +6NS CPs*	*KF+6_DOM2 vs. other +6_DOM2 CPs*	*KF vs. other 00Z CPs*
KF+6	29	97	-	41	-	-	-
BMJ+6	202	73	350	57	429	320	562
G3+6	125	144	32	287	74	359	464
TD+6	143	45	40	65	78	96	126
AVERAGE	124	89	237	112	193	258	384

Table 4 Megi landfall distance differences for each CP. NB: * indicates the G3/G3+6 cases did not make landfall. In this instance we compare the position at the time of the first storm making landfall (KF)

Case	*vs. +6*	*vs. DOM2*	*KF vs. other CPs*	*vs. NS CP*	*KF NS vs. other NS CPs*	*KF_DOM2 vs. other DOM2 CPs*	*KF+6 vs. other +6 CPs*
KF	53	74	-	10	-	-	-
BMJ	45	73	183	2	189	200	188
G3	249*	248*	581*	343	289	793*	718*
TD	34	113	251	100	160	212	260
AVERAGE	95	127	338	113	212	401	388

Table 5 Comparison of the landfall of each simulation to the observed landfall for each of the cyclone cases. *These Rita cases were '+6'. N/A indicates no landfall. †Indicates the average is only based on two cases due to a simulation not making landfall in one of the cases

Case	*Yasi vs. observed landfall (km)*	*Rita vs. observed landfall (km)*	*Megi vs. observed landfall (km)*	*Average (from all three cases)*
KF	173	291	262	242
BMJ	490	301	78	289
G3	445	192	N/A	318†
TD	80	165	14	86
KF+6	158	268	306	244
BMJ+6	373	98	122	197
G3+6	364	66	N/A	215†
TD+6	75	307	46	142
KF_NS	188	301*	270	253
BMJ_NS	475	153*	81	236
G3_NS	170	236*	26	144
TD_NS	117	373*	110	200
KF_DOM2	233	170*	328	243
BMJ_DOM2	415	154*	145	244
G3_DOM2	408	211*	N/A	309†
TD_DOM2	89	266*	122	159

Table 6 Matrix of simulated TC motion (TC motion from the vector plots) and the diagnosed motion derived from the WN-1 PVT plots, for the Yasi case

Scheme and analysis period	*Simulated direction (TC motion)*	*Diagnosed direction (WN-1 PVT)*	*Disagreement*
KF (12 – 18)	260°	147°	113°
BMJ (12 – 18)	223°	230°	7°
KF (18 – 24)	255°	196°	59°
BMJ (18 – 24)	246°	216°	30°
KF (36 – 42)	250°	190°	60°
BMJ (36 – 42)	218°	235°	17°
KF (42 – 48)	245°	210°	35°
BMJ (42 – 48)	236°	242°	6°
G3 (36 – 42)	238°	224°	14°
G3_NS (36 – 42)	251°	204°	47°
G3 (42 – 48)	234°	225°	9°
G3_NS (42 – 48)	245°	205°	40°
G3 (48 – 54)	228°	227°	1°
G3_NS (48 – 54)	237°	190°	47°
G3 (54 – 60)	237°	218°	19°
G3_NS (54 – 60)	247°	175°	72°

Table 7 The same as Table 6, for the Rita case

Scheme and analysis period	*Simulated direction (TC motion)*	*Diagnosed direction (WN-1 PVT)*	*Disagreement*
KF+6 (24 – 30)	276°	264°	12°
BMJ+6 (24 – 30)	264°	263°	1°
KF+6 (30 – 36)	288°	270°	18°
BMJ+6 (30 – 36)	276°	257°	19°
KF+6 (36 – 42)	279°	270°	9°
BMJ+6 (36 – 42)	254°	246°	8°
KF+6 (42 – 48)	285°	284°	1°
BMJ+6 (42 – 48)	267°	250°	17°
G3+6 (30 – 36)	297°	282°	15°
G3+6_NS (30 – 36)	280°	266°	14°
G3+6 (42 – 48)	287°	297°	10°
G3+6_NS (42 – 48)	278°	269°	9°
G3+6 (60 – 66)	301°	289°	12°
G3+6_NS (60 – 66)	277°	284°	7°

1349 **Table 8** The same as Table 6, for the Megi case.

Scheme and analysis period	*Simulated direction (TC motion)*	*Diagnosed direction (WN-1 PVT)*	*Disagreement*
KF (42 – 48)	302°	293°	9°
BMJ (42 – 48)	327°	285°	42°
KF (48 – 54)	299°	286°	13°
BMJ (48 – 54)	315°	286°	29°
KF (72 – 78)	275°	278°	3°
BMJ (72 – 78)	241°	226°	15°
KF (96 – 102)	253°	264°	11°
BMJ (96 – 102)	330°	319°	11°
G3 (48 – 54)	270°	280°	10°
G3_NS (48 – 54)	302°	290°	12°
G3 (54 – 60)	304°	300°	4°
G3_NS (54 – 60)	289°	286°	3°
G3 (84 – 90)	295°	292°	3°
G3_NS (84 – 90)	268°	273°	5°
G3 (90 – 96)	297°	292°	5°
G3_NS (90 – 96)	276°	277°	1°
G3 (96 – 102)	291°	287°	4°
G3_NS (96 – 102)	259°	257°	2°
G3 (102 – 108)	311°	292°	19°
G3_NS (102 – 108)	252°	257°	5°
G3 (120 – 126)	28°	43°	14°
G3 (138 – 144)	31°	24°	7°

1350

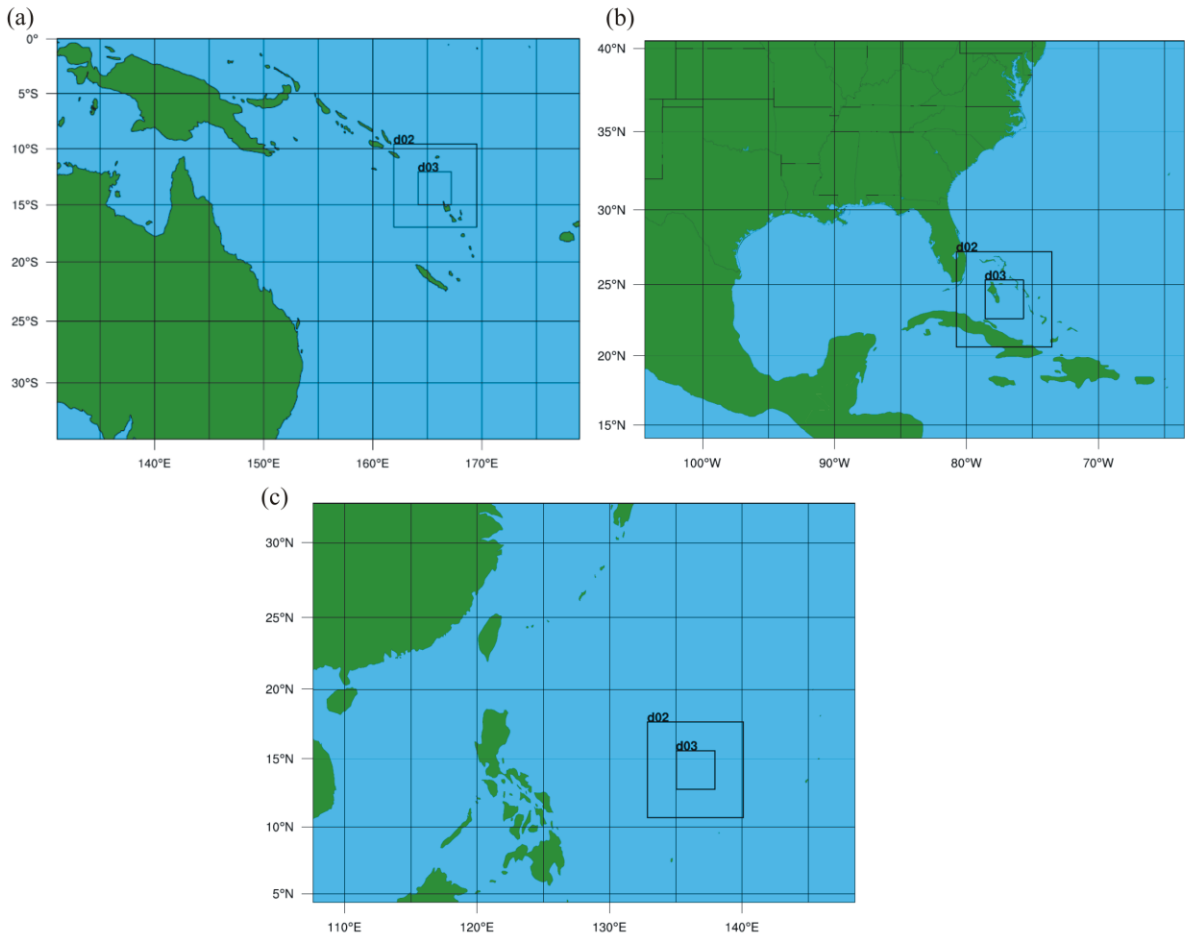

(a)
0°
5°S
10°S
15°S
20°S
25°S
30°S
140°E
150°E
160°E
170°E
d02
d03
(b)
40°N
35°N
30°N
25°N
20°N
15°N
100°W
90°W
80°W
70°W
d02
d03
(c)
30°N
25°N
20°N
15°N
10°N
5°N
110°E
120°E
130°E
140°E
d02
d03

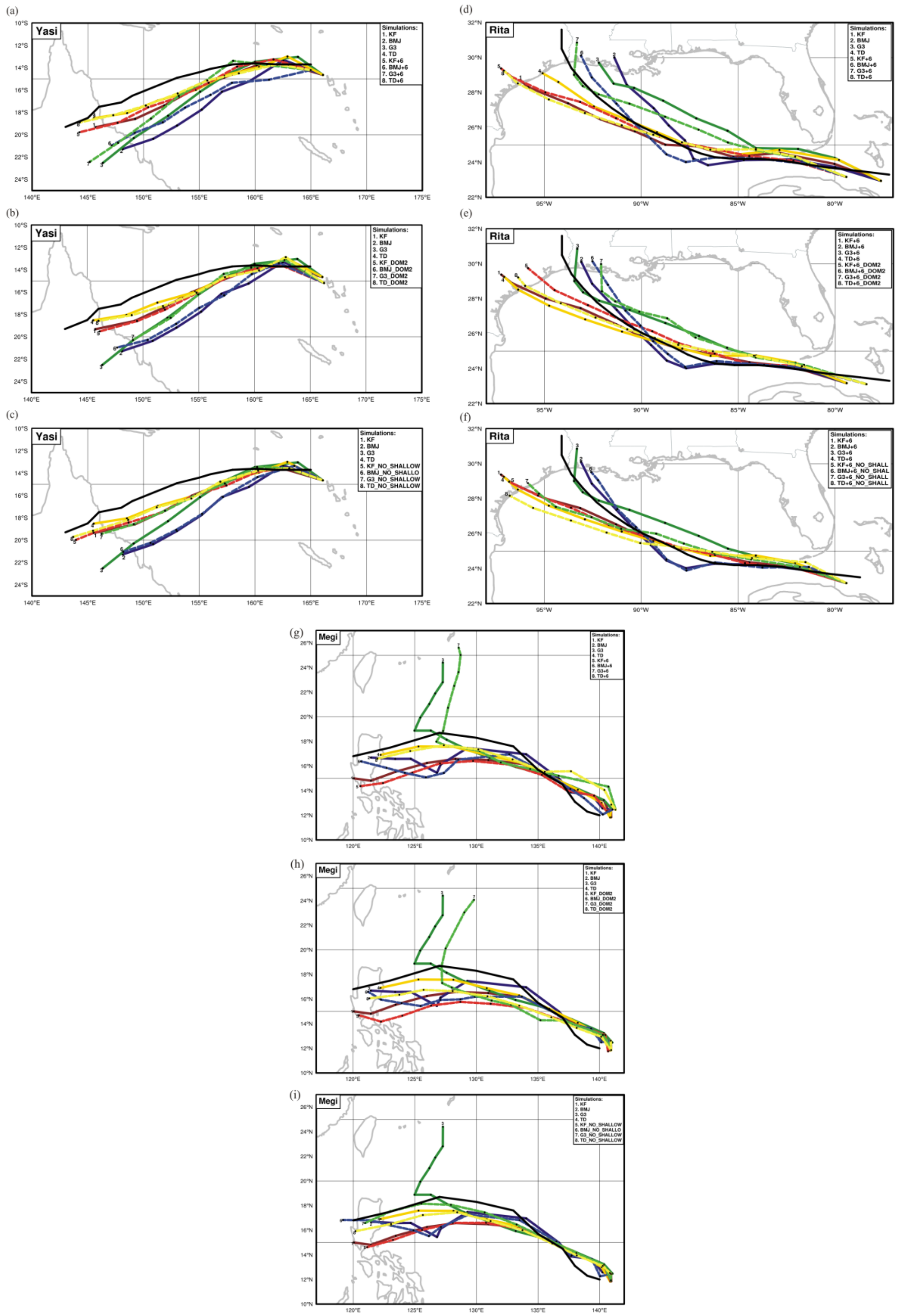

(a)
Yasi
Simulations:
1. KF
2. BMJ
3. G3
4. TD
5. KF+6
6. BMJ+6
7. G3+6
8. TD+6
(b)
Yasi
Simulations:
1. KF
2. BMJ
3. G3
4. TD
5. KF_DOM2
6. BMJ_DOM2
7. G3_DOM2
8. TD_DOM2
(c)
Yasi
Simulations:
1. KF
2. BMJ
3. G3
4. TD
5. KF_NO_SHALLOW
6. BMJ_NO_SHALLO
7. G3_NO_SHALLOW
8. TD_NO_SHALLOW
(d)
Rita
Simulations:
1. KF
2. BMJ
3. G3
4. TD
5. KF+6
6. BMJ+6
7. G3+6
8. TD+6
(e)
Rita
Simulations:
1. KF+6
2. BMJ+6
3. G3+6
4. TD+6
5. KF+6_DOM2
6. BMJ+6_DOM2
7. G3+6_DOM2
8. TD+6_DOM2
(f)
Rita
Simulations:
1. KF+6
2. BMJ+6
3. G3+6
4. TD+6
5. KF+6_NO_SHALL
6. BMJ+6_NO_SHAL
7. G3+6_NO_SHALL
8. TD+6_NO_SHALL
(g)
Megi
Simulations:
1. KF
2. BMJ
3. G3
4. TD
5. KF+6
6. BMJ+6
7. G3+6
8. TD+6
(h)
Megi
Simulations:
1. KF
2. BMJ
3. G3
4. TD
5. KF_DOM2
6. BMJ_DOM2
7. G3_DOM2
8. TD_DOM2
(i)
Megi
Simulations:
1. KF
2. BMJ
3. G3
4. TD
5. KF_NO_SHALLOW
6. BMJ_NO_SHALLO
7. G3_NO_SHALLOW
8. TD_NO_SHALLOW

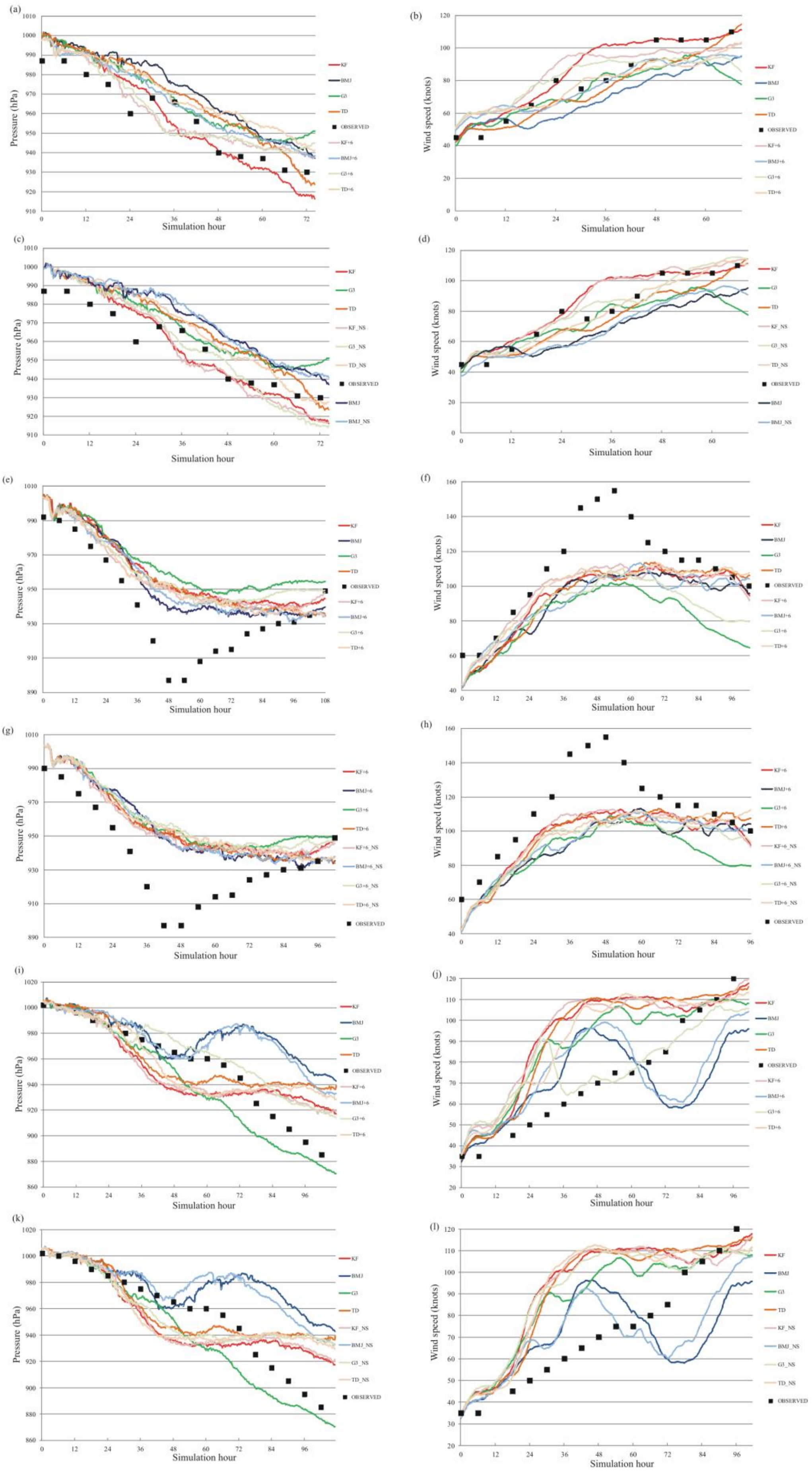
(a)
Pressure (hPa)
Simulation hour
KF
BMJ
G3
TD
OBSERVED
KF+6
BMJ+6
G3+6
TD+6
(b)
Wind speed (knots)
Simulation hour
(c)
Pressure (hPa)
Simulation hour
KF_NS
G3_NS
TD_NS
BMJ_NS
(d)
Wind speed (knots)
Simulation hour
(e)
Pressure (hPa)
Simulation hour
(f)
Wind speed (knots)
Simulation hour
(g)
Pressure (hPa)
Simulation hour
KF+6_NS
BMJ+6_NS
G3+6_NS
TD+6_NS
(h)
Wind speed (knots)
Simulation hour
(i)
Pressure (hPa)
Simulation hour
(j)
Wind speed (knots)
Simulation hour
(k)
Pressure (hPa)
Simulation hour
(l)
Wind speed (knots)
Simulation hour

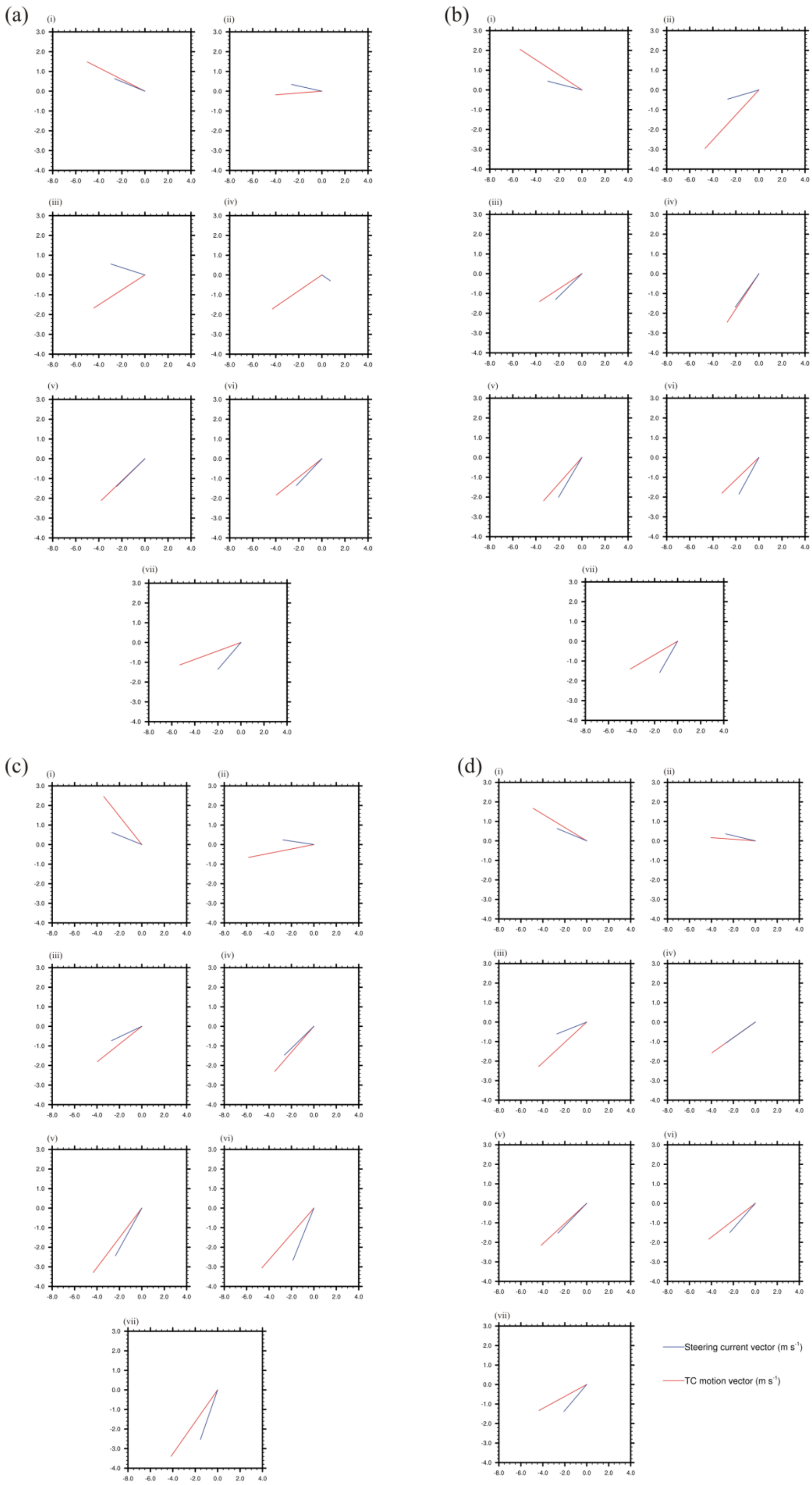
(a)
(i)
(ii)
(iii)
(iv)
(v)
(vi)
(vii)
(b)
(c)
(d)
Steering current vector (m s^{-1})
TC motion vector (m s^{-1})

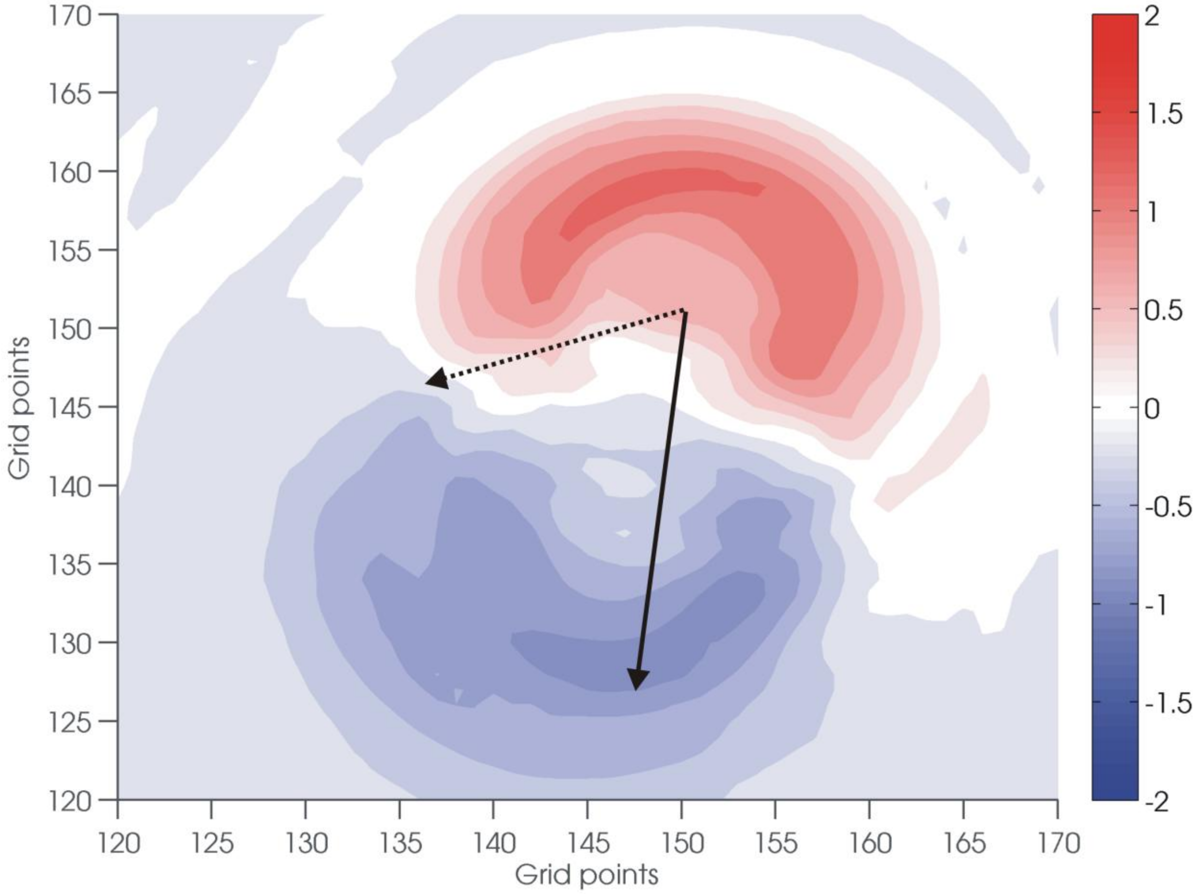
Grid points
Grid points
170
165
160
155
150
145
140
135
130
125
120
120
125
130
135
140
145
150
155
160
165
170
2
1.5
1
0.5
0
-0.5
-1
-1.5
-2

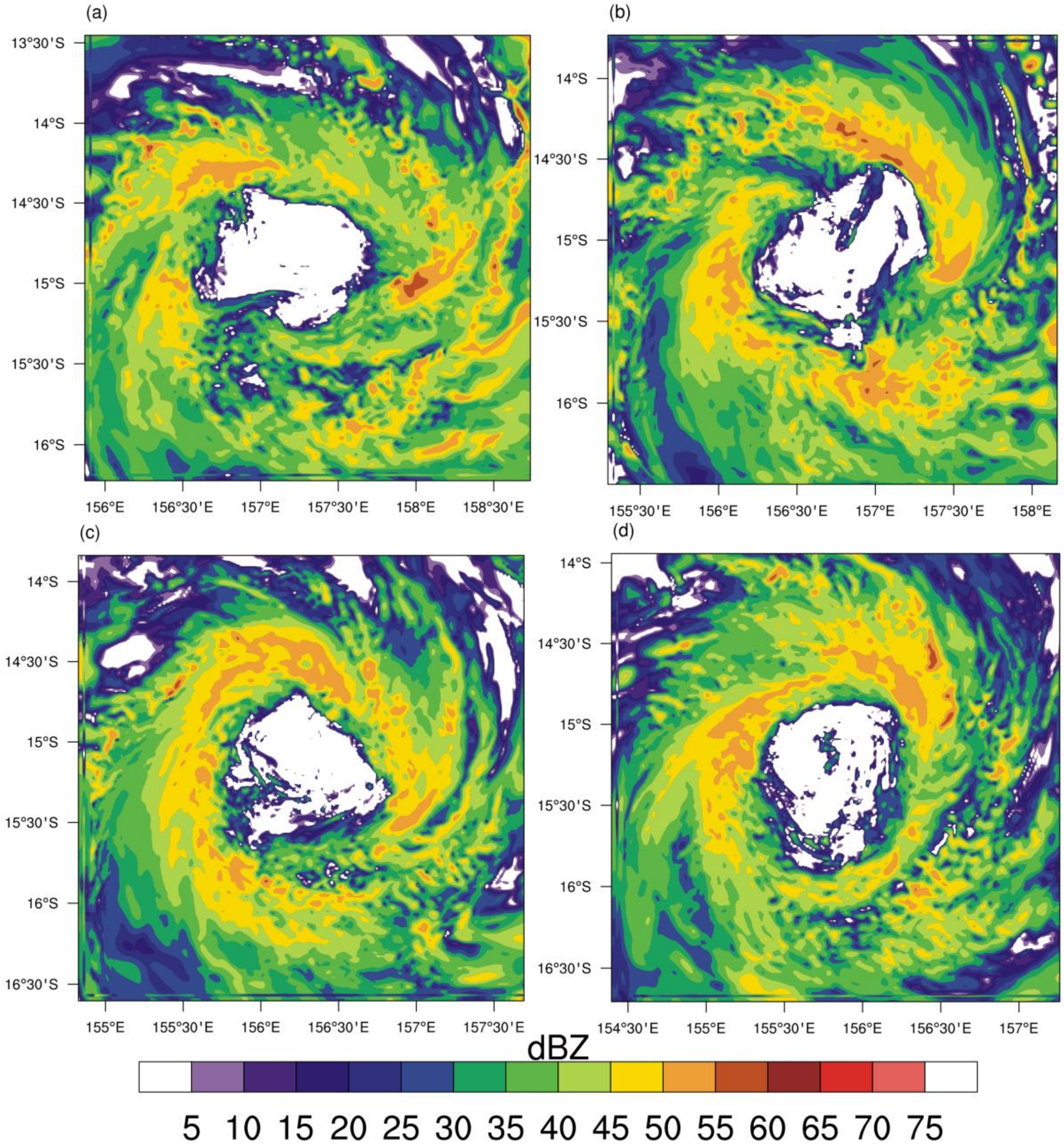
(a)
(b)
(c)
(d)
13°30'S
14°S
14°30'S
15°S
15°30'S
16°S
16°30'S
154°30'E
155°E
155°30'E
156°E
156°30'E
157°E
157°30'E
158°E
158°30'E
dBZ
5 10 15 20 25 30 35 40 45 50 55 60 65 70 75

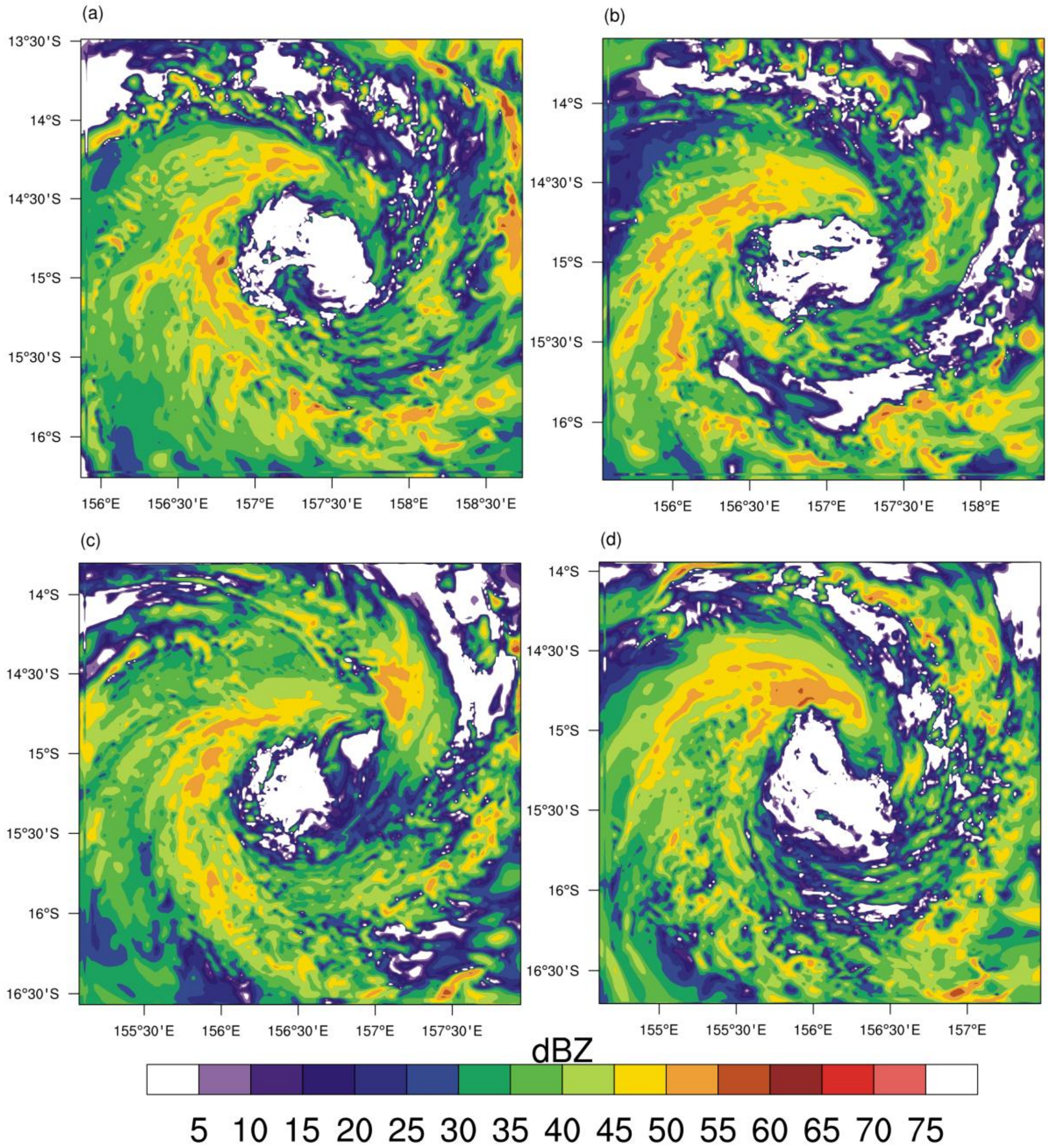
(a)
(b)
(c)
(d)
13°30'S
14°S
14°30'S
15°S
15°30'S
16°S
16°30'S
155°E
155°30'E
156°E
156°30'E
157°E
157°30'E
158°E
158°30'E
dBZ
5 10 15 20 25 30 35 40 45 50 55 60 65 70 75

1357

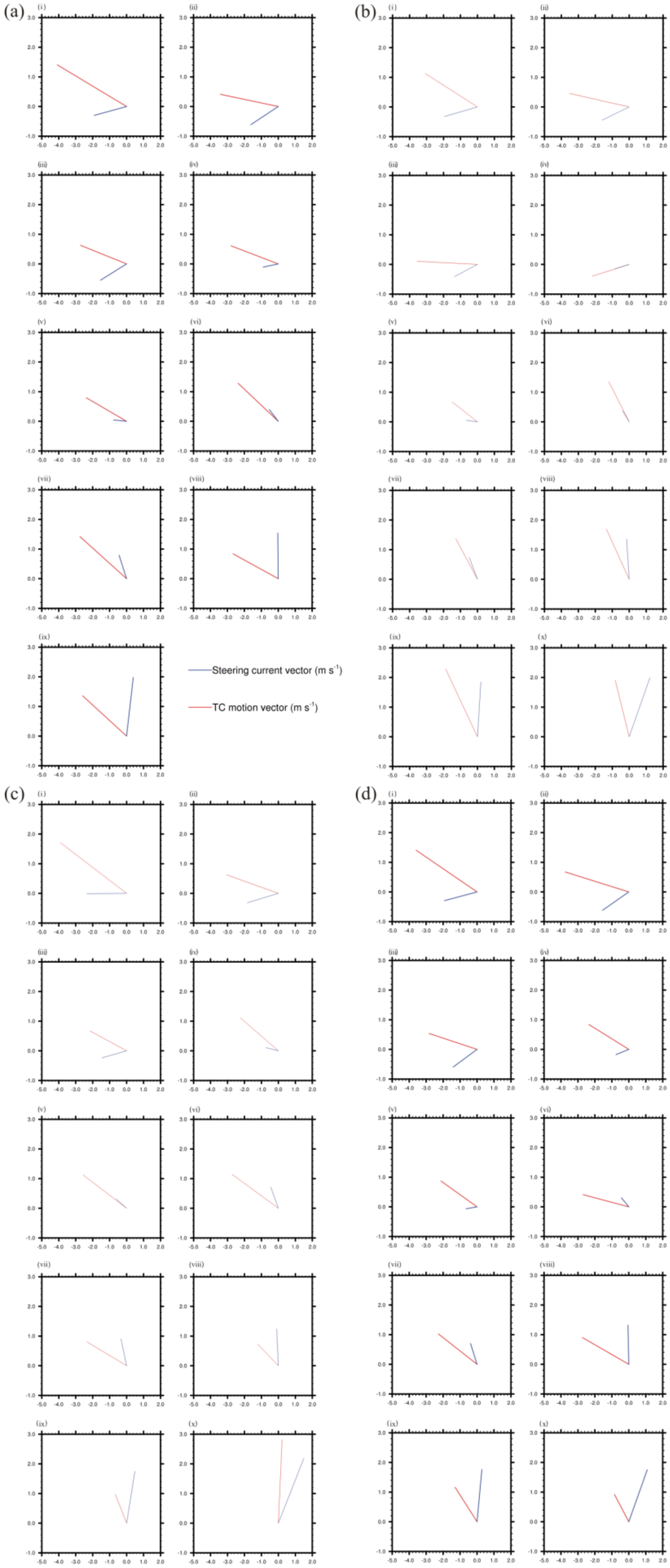
(a)
(b)
(c)
(d)
Steering current vector (m s-1)
TC motion vector (m s-1)

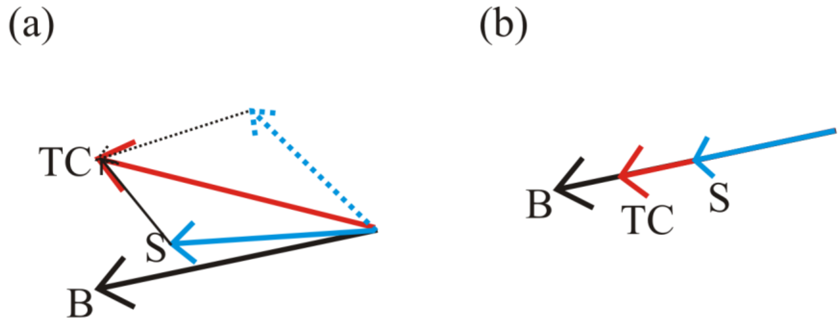
(a)
(b)
TC
S
B
B
TC
S

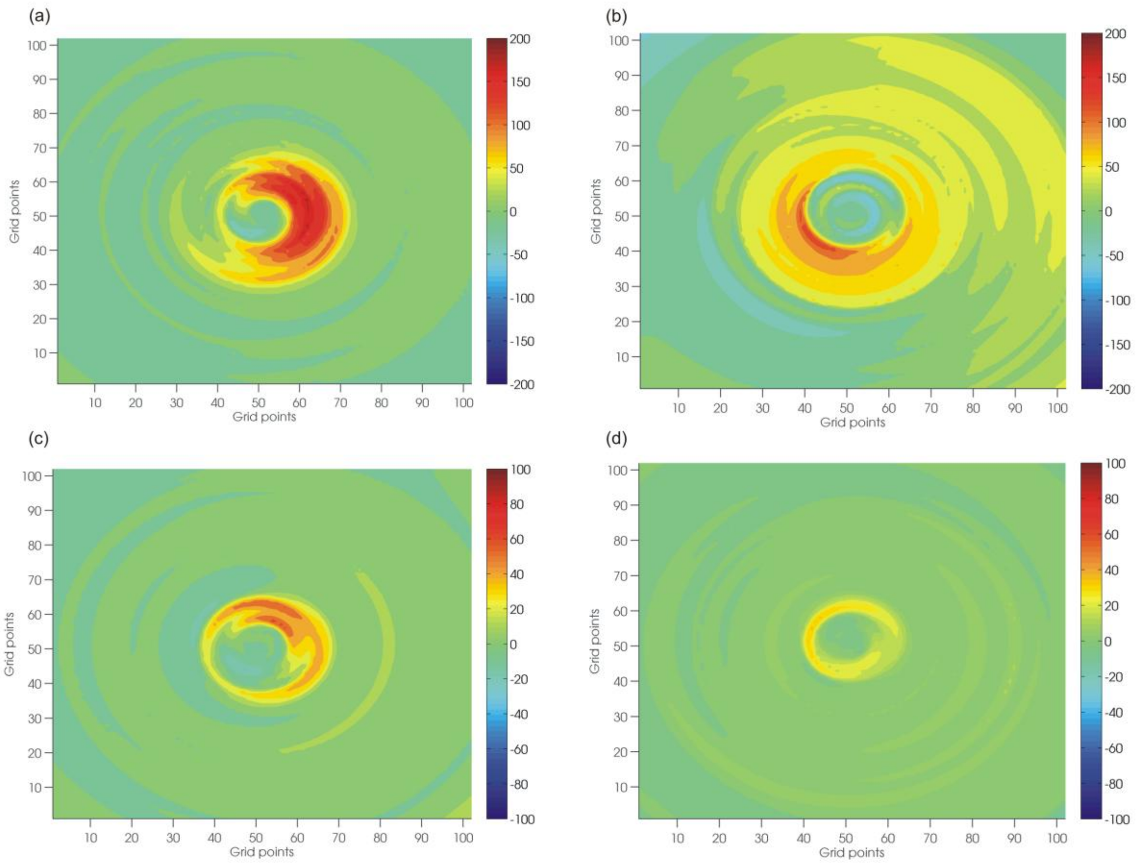
(a)
(b)
(c)
(d)
Grid points
Grid points
Grid points
Grid points
Grid points
Grid points
Grid points
Grid points

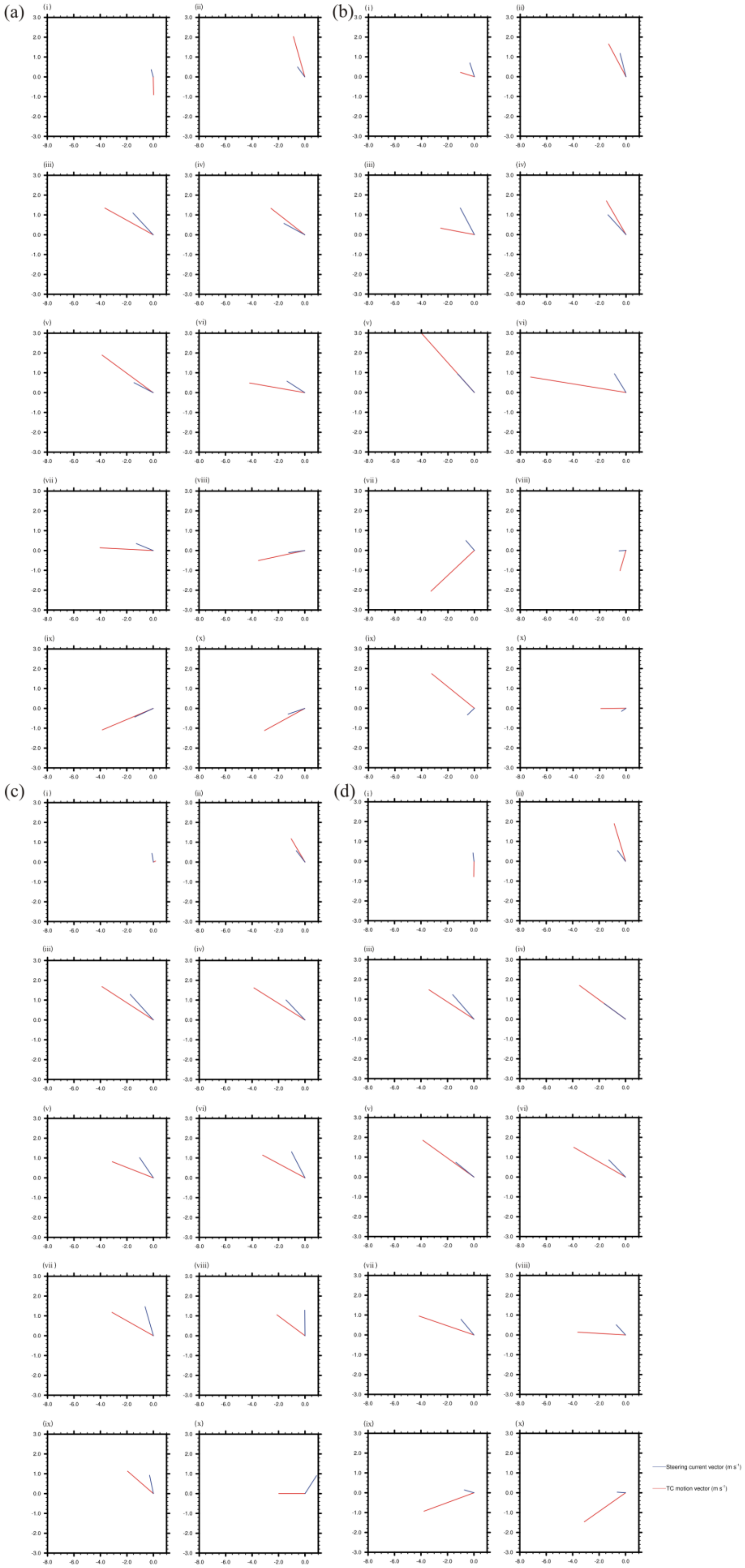
(a)
(b)
(c)
(d)
(i)
(ii)
(iii)
(iv)
(v)
(vi)
(vii)
(viii)
(ix)
(x)
Steering current vector (m s^{-1})
TC motion vector (m s^{-1})

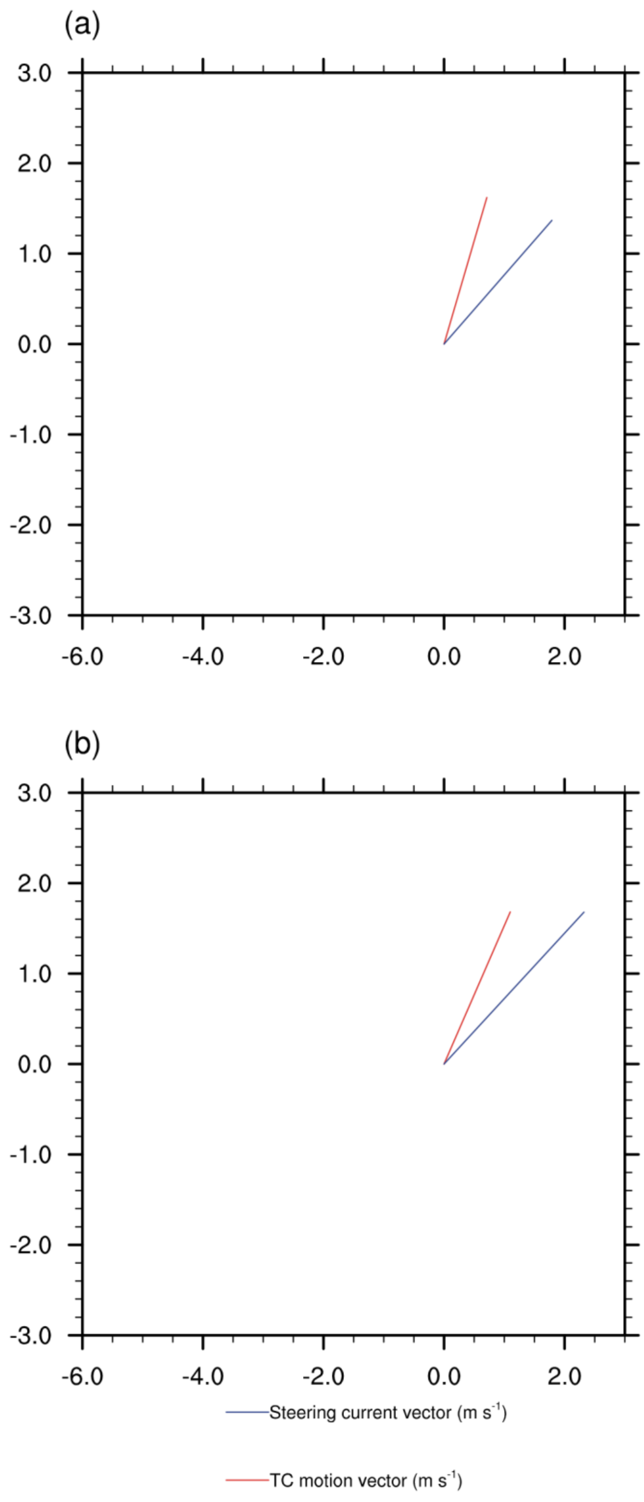
(a)
3.0
2.0
1.0
0.0
-1.0
-2.0
-3.0
-6.0
-4.0
-2.0
0.0
2.0
(b)
3.0
2.0
1.0
0.0
-1.0
-2.0
-3.0
-6.0
-4.0
-2.0
0.0
2.0
Steering current vector (m s-1)
TC motion vector (m s-1)

1362

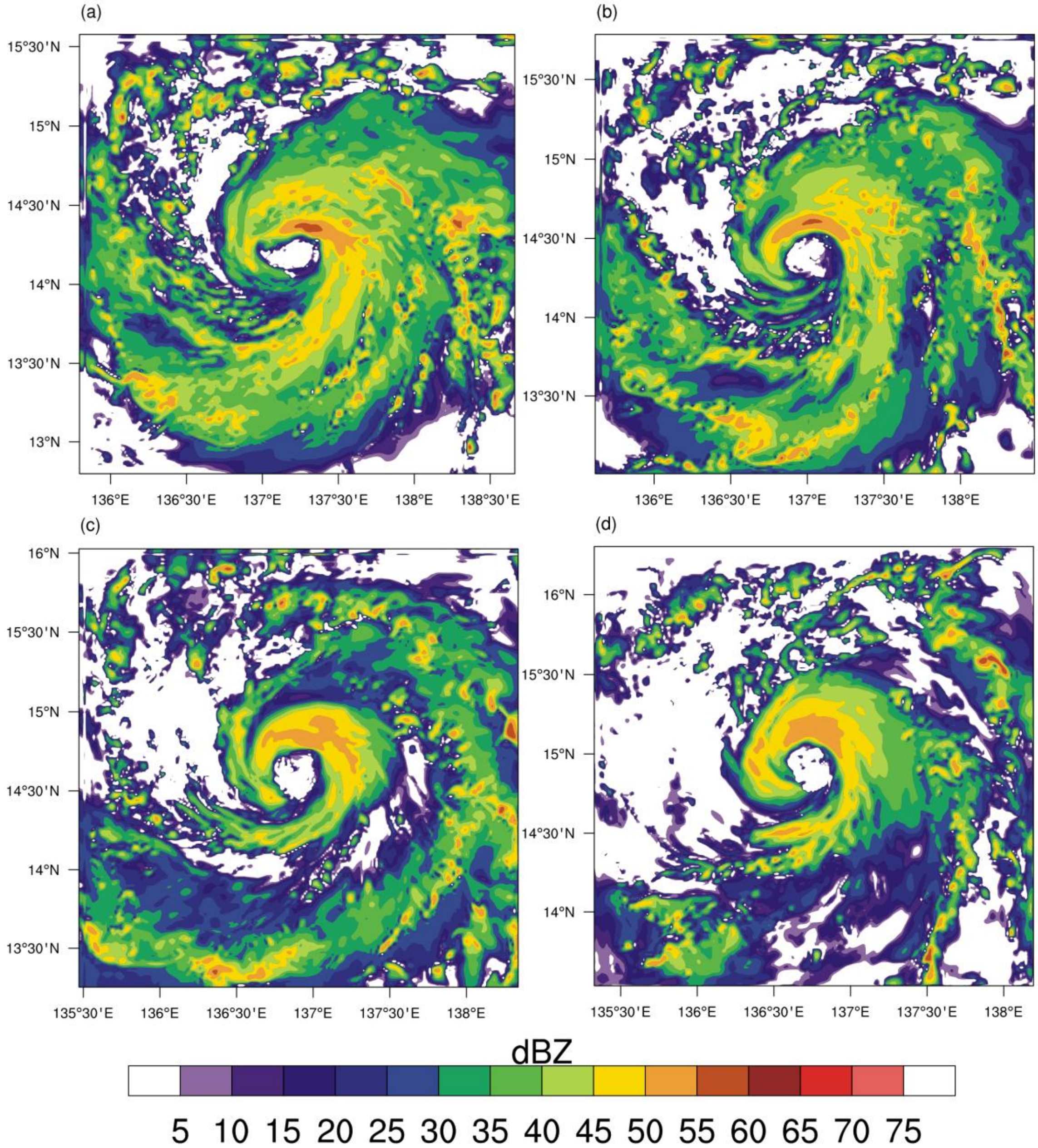
(a)
(b)
(c)
(d)
15°30'N
15°N
14°30'N
14°N
13°30'N
13°N
16°N
135°30'E
136°E
136°30'E
137°E
137°30'E
138°E
138°30'E
dBZ
5 10 15 20 25 30 35 40 45 50 55 60 65 70 75

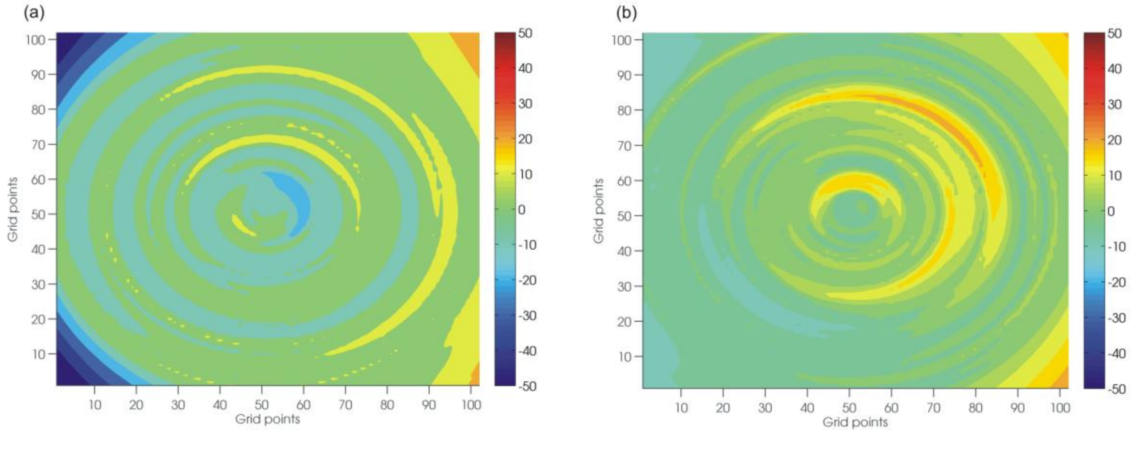
(a)
(b)
Grid points
Grid points
10 20 30 40 50 60 70 80 90 100
50 40 30 20 10 0 -10 -20 -30 -40 -50